JOURNAL OF THE ROYAL SOCIETY Interface

J. R. Soc. Interface (2009) **6**, 1005–1025
doi:10.1098/rsif.2008.0492
Published online 20 January 2009

Passive versus active engulfment: verdict from trajectory simulations of lunge-feeding fin whales *Balaenoptera physalus*

J. Potvin[1,*], J. A. Goldbogen[2] and R. E. Shadwick[2]

[1]*Department of Physics, Saint Louis University, 3450 Lindell Boulevard, Saint Louis, MO 63103, USA*
[2]*Department of Zoology, University of British Columbia, 6270 University Boulevard, Vancouver, British Columbia, Canada V6T 1Z4*

Lunge-feeding in rorqual whales represents the largest biomechanical event on Earth and one of the most extreme feeding methods among aquatic vertebrates. By accelerating to high speeds and by opening their mouth to large gape angles, these whales generate the water pressure required to expand their mouth around a large volume of prey-laden water. Such large influx is facilitated by highly extensible ventral groove blubber (VGB) associated with the walls of the throat (buccal cavity). Based on the mechanical properties of this tissue, previous studies have assumed lunge-feeding to be an entirely passive process, where the flow-induced pressure driving the expansion of the VGB is met with little resistance. Such *compliant engulfment* would be facilitated by the compliant properties of the VGB that have been measured on dead specimens. However, adjoining the ventral blubber are several layers of well-developed muscle embedded with mechanoreceptors, thereby suggesting a capability to gauge the magnitude of engulfed water and use eccentric muscle action to control the flux of water into the mouth. An unsteady hydrodynamic model of fin whale lunge-feeding is presented here to test whether engulfment is exclusively passive and compliant or involves muscle action. The model is based on the explicit simulation of the engulfed water as it interacts with the buccal cavity walls of the whale, under different heuristically motivated cavity forces. Our results, together with their comparison with velocity data collected in the field, suggest that adult rorquals actively push engulfed water forward from the very onset of mouth opening in order to successfully complete a lunge. Interestingly, such an action involves a *reflux* of the engulfed mass rather than the oft-assumed *rebound*, which would occur mainly at the very end of a lunge sequence dominated by compliant engulfment. Given the great mass of the engulfed water, reflux creation adds a significant source of hydrodynamic drag to the lunge process, but with the benefit of helping to circumvent the problem of removing prey from baleen by enhancing the efficiency of cross-flow filtration after mouth closing. Reflux management for a successful lunge will therefore demand well-coordinated muscular actions of the tail, mouth and ventral cavity.

Keywords: lunge-feeding; hydrodynamics; rorqual whales

1. INTRODUCTION

Most adept swimming and flying animals are well streamlined in order to reduce drag and enhance locomotor efficiency. However, many marine vertebrates, including fishes, birds and whales, need dynamic water pressure, or in other words *drag*, to power bulk filter-feeding mechanisms, and therefore represent a paradox in functional morphology that has largely been ignored. Rorquals are a family of exceptionally streamlined baleen whales (Mysticeti: Balaenopteridae) that exhibit a type of ram-feeding strategy (lunge-feeding) that is considered the largest biomechanical event on Earth (Brodie 1993). During engulfment, massive amounts of prey and water are engulfed and filtered intermittently either at the sea surface or multiple times during a foraging dive (Goldbogen *et al.* 2006, 2007, 2008).

Recent deployments of high-resolution digital tags on foraging rorquals have prompted new studies on the physiology and ecology of lunge-feeding, particularly because of the accurate kinematic data obtained from the lunge-feeding whales in their natural environment (Goldbogen *et al.* 2006). These tags demonstrated that rorqual foraging dives typically involve multiple lunges at depth directed at dense aggregations of zooplankton (Calambokidis *et al.* 2008; Goldbogen *et al.* 2008). Despite the ability to dive over 400 m to feed (Panigada *et al.* 1999), rorquals exhibit severely limited dive

*Author for correspondence (potvinj@slu.edu).

Received 17 November 2008
Accepted 16 December 2008

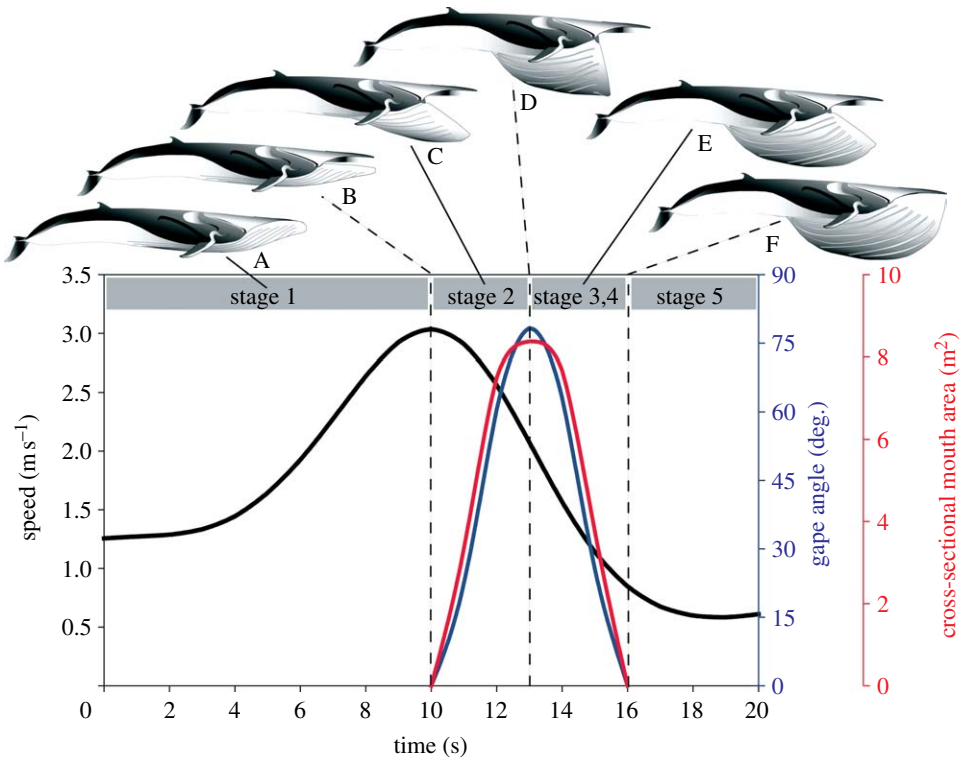

Figure 1. Kinematics of a fin whale *Balaenoptera physalus* lunge. The schematic shows the different stages of engulfment and the expansion of the VGB. Average speed of the body (black line) was calculated at 1 Hz from high-resolution digital tag data (50 lunges and 7 whales). Changes in gape angle (blue line) and how it controls the projected frontal area of the mouth (red line) are shown as a function of time from mouth opening (B; $t=10$ s), to maximum gape (D; $t=13$ s), to mouth closure (F; $t=16$ s). These landmark events define the stages of engulfment: pre-engulfment acceleration (A, stage 1); mouth opening and initial engulfment (C, stage 2); onset of mouth closure and continued engulfment (E, stage 3); mouth closure and pre-purging (E, stage 4); and purging (stage 5). Adapted from Goldbogen *et al.* (2007).

durations that contradict allometric trends of enhanced diving capacity that accompany larger body sizes (Croll *et al.* 2001; Halsey *et al.* 2006). The purported high energetic cost of foraging, because of the high drag experienced during lunge-feeding, is thought to be the proximate cause of these limited dive times (Acevedo-Gutierrez *et al.* 2002).

It is unknown how much energy is needed to successfully execute a lunge, largely because the detailed forces and mechanisms that drive lunge-feeding are also unknown. Energy expenditure will be time dependent given the unsteady nature of lunge-feeding, as the whale imparts its momentum to the engulfed water. Such a collision between lunging whale and engulfed water requires a complete assessment of the forces at play, generated not only by the whale but also by the fluid mass that interacts with it. The latter is important given the large sizes of adult rorqual whales, which range from 7 m in minke whales to over 30 m in blue whales (Lockyer 1976). Here, large fluxes of water into the mouth are accommodated by the relaxation and stretching of the ventral groove blubber (VGB), which includes layers of muscle tissue and together comprise the throat pouch or buccal cavity (Orton & Brodie 1987).

Engulfment involves longitudinal and circumferential extension of the VGB similar to an unfurling parachute (figure 1) and, with the apparent disarticulation of the jaw itself (Lambertsen *et al.* 1995), is a process that enhances the frontal surface area of the mouth at large gape angles. Because it extends from the tip of the lower jaw to the umbilicus and, at the same time, is so extensible (Orton & Brodie 1987), the VGB spans more than 50 per cent of a rorqual whale's body length, thereby yielding an extraordinary capacity for large engulfment volumes. This is enabled through ontogeny, where rorquals undergo a dramatic increase in body size (Lockyer 1981; Brown & Lockyer 1984) and a massive reduction in their tongue musculature as an adaptation to facilitate extreme distension of the oral cavity during lunge-feeding (Pivorunas 1977; Werth 2007). As a result, the weakly muscularized tongue is inverted ventrally during engulfment, thereby forming a capacious sac that is accommodated by the extensible VGB (Lambertsen 1983). From a physical point of view, the extreme size of the buccal cavity implies that enough fluid can be engulfed to nearly double the mass of a lunging whale. Therefore, the speeds of the latter and of the engulfed water may change substantially over time, as determined by the balance, or lack thereof, of the forces that the whale and engulfed mass apply on each other.

Here, we present a model named the *basic lunge-feeding model* (BLFm), which constitutes a first-ever attempt at modelling explicitly the unsteady nature of flow generated during engulfment. This approach will involve all forces of the lunge-feeding process, including buoyancy, thrust, drag, as well as potential muscle

action within the buccal cavity. These forces are resolved to predict the trajectories of lunging whale and engulfed water as they collide. Also, the model determines the amount of drag required to engulf a given volume of water as a function of time. The BLFm improves on an earlier attempt based on integrating kinematic and morphological data into a simple quasi-steady hydrodynamic model of lunge-feeding (Goldbogen *et al.* 2007), to show a link between the drag required to expand the buccal cavity and the resulting engulfed water volume. But that approach did not make explicit enough those unsteady hydrodynamic phenomena that undoubtedly dominate this complex process. Furthermore, those authors assumed that engulfment is entirely passive and that the VGB could expand without limit to accommodate incoming water fluxes, as traditionally portrayed in previous studies (Lambertsen 1983; Orton & Brodie 1987).

This study challenges the long-held, but never tested, assumption that lunge-feeding is entirely compliant by simulating different types of buccal cavity wall forces. In fact, we predict that lunge-feeding is not a passive process, but rather a dynamical one where rorquals use eccentric muscle contraction to slowly push water forward over the course of the lunge. This is important because, by virtue of Newton's third law of motion, any internal muscular action used to control the flux of water into the mouth will give rise to another source of hydrodynamic drag (the opposing force) in addition to that related to the flow about the animal's body.

Our hypothesis is based on morphological information, behavioural observations and hydrodynamic principles. First, the floor of the buccal cavity is composed of several well-developed muscle layers (Orton & Brodie 1987; Pivorunas 1977) that are embedded with mechanoreceptors (deBakker *et al.* 1997). Such a mechanical design implies that rorquals may be able to gauge the cumulative magnitude of water during engulfment, and, consequently, develop sufficient muscle force that is proportional to that water mass. Second, observations of lunges at the sea surface typically show a relatively small volume of water exiting the mouth at high speed near the end of the lunge, which is suggestive of active engulfment. Third, because force is required to stretch the VGB (Orton & Brodie 1987) and hydrodynamic drag can provide such a force (Goldbogen *et al.* 2007), water must be pushed forward (and around the mouth) because this is precisely how drag is generated (Vogel 1994).

Our simulations of active (or dynamic) engulfment more accurately predict the trajectory (body speed as a function of time) of actual lunge-feeding whales, compared with passive engulfment simulations that show: (i) premature filling of the buccal cavity and (ii) unrealistic forces imposed on the engulfment apparatus. Interestingly, the active engulfment models that best fit current digital tag data do suggest the existence of *engulfed mass reflux* due to the gradual shoving of water from the very onset of mouth opening. The concept of reflux is important for thoroughly understanding the efficiency of a lunge, given the large fluid mass involved and the changes on a whale's speed that ensue. Too fast of a reflux (compared to instantaneous whale speed) will cause some of the engulfed mass to re-exit the buccal cavity, perhaps much sooner than actual mouth-closing, in essence wasting the energy spent in engulfment. Too slow of a reflux, on the other hand (as with compliant engulfment), will require unrealistic muscle force at the end of a lunge to bring the engulfed mass to the speed of the whale at that moment. Therefore, a successful lunge demands well-coordinated tail, mouth and ventral muscular actions that yield not only an optimum engulfed mass by the time of mouth closure, but also gradual forward motion of the latter in order to facilitate purging. Such internal flow should enhance the efficiency of cross-flow filtration and help circumvent the problem of removing prey from baleen.

2. PRINCIPLES AND APPROXIMATIONS

2.1. Engulfment stages

The BLFm describes the engulfment process with four distinct stages (figure 1): pre-engulfment acceleration (stage 1); mouth opening and initial engulfment (stage 2); onset of mouth closure and continued engulfment (stage 3); and mouth closure and pre-purging (stage 4). Kinematic data (Goldbogen *et al.* 2006) indicate that, prior to a lunge, the whale accelerates with its mouth closed to a given speed while under the propulsion generated by the tail and against the resistive effects of drag. During the lunge, water is engulfed as the animal moves forward by its own propulsion, accompanied by a concomitant deceleration despite continued swimming (Goldbogen *et al.* 2006). The hydrodynamic pressure generated from swimming expands the buccal cavity (Orton & Brodie 1987; Goldbogen *et al.* 2007) while simultaneously the engulfed water is pushed forward by the posterior end of the buccal cavity (figure 2). The reaction to such an action can be seen as an extra source of drag that will cause further deceleration of the whale beyond what is usually contributed by drag due to the flow around the body. Given the appropriate cavity wall force, the engulfed water will gain speed relative to surrounding water and in the same direction as the whale's own motion, thereby giving rise to reflux. In other words, the cavity wall force will be the very agent that transfers the kinetic energy of the whale to the engulfed water.

Engulfment continues during the onset of mouth closure (stage 3), where the engulfed water mass increases speed and the whale loses speed. For these reasons, it is possible that the speed of the engulfed water (relative to the shore) will become greater than that of the whale (also measured with respect to the shore) at the very end of the lunge. It is at this point that stage 4 begins, where a small amount of water may exit the mouth, but with most of the engulfed water remaining within and possibly rebounding within the cavity (figure 3). Rebounding waves within the buccal cavity have been observed for several rorqual species lunge-feeding at the sea surface (Kot 2005) as well as underwater (Bryde's whale lunges; BBC Blue Planet: Open Ocean Chapter). Although counter-intuitive, it is

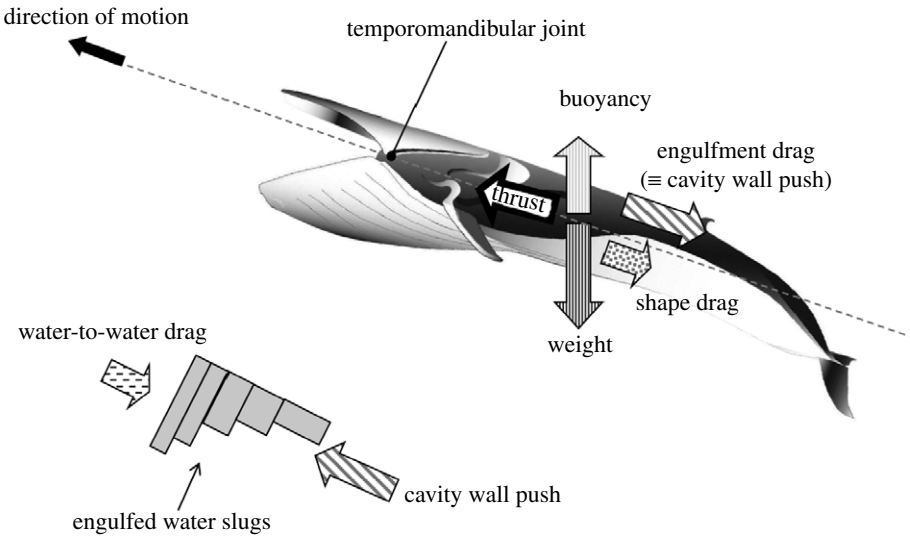

Figure 2. Force diagram of a lunging fin whale *Balaenoptera physalus* and engulfed water.

believed that the rebounding wave could increase the efficiency of filtration via a cross-flow mechanism during the purging phase (Goldbogen *et al.* 2007).

The BLFm divides the mouth closing and pre-purging stage into two substages (figure 3), to distinguish the *bulk ejection* substage (stage 4.1) from the *partial ejection* substage (stage 4.2). In stage 4.2, the portion of the buccal cavity wall ventral to the mandible is largely vertical, thus offering an obstacle to the exiting water. By contrast, stage 4.1 (the earlier stage) depicts the buccal cavity wall at a more shallow angle. From the point of view of buccal cavity wall forces, the engulfed water in stage 4.1 is still being pushed, for the most part, by the same type of force that originated from the posterior end of the ventral cavity during stages 2 and 3. During partial ejection (stage 4.2), such a push is now resisted by the vertical wall of the buccal cavity, to effectively block the forward motion of the engulfed volume located ventral to the mandible. The retained water now becomes part of the decelerating whale, while the water above the mandible is pushed out as a single body by the same reactive forces derived from the posterior end of the buccal cavity.

In its current implementation, the BLFm will not include the simulation of the purging stage that follows mouth closure, being purely an internal process generally invisible to the kinematics measured by the digital tags. Moreover, purging in baleen whales is still an uncharacterized process that merits further investigation, especially in the fluid dynamics laboratory. Finally, the modelling discussed in this paper will only address the types of feeding lunges that are completely performed underwater, either vertically or horizontally, and leave the consideration of surface lunging to another publication.

2.2. External versus internal flows; two-component drag

The BLFm explicitly defines a distinction between the so-called 'external flows' and 'internal flows' (figure 4).

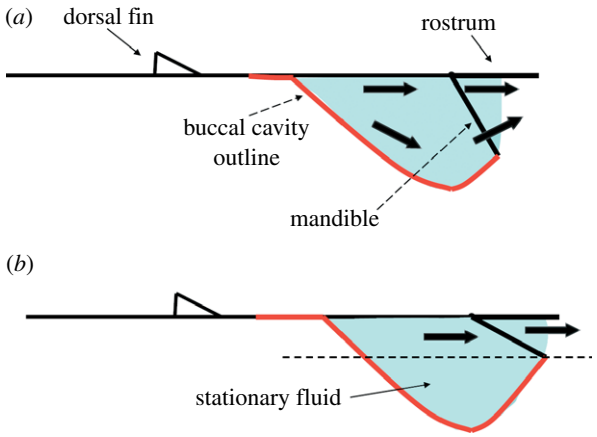

Figure 3. Engulfed slug train shape and buccal cavity contour during mouth closing: (*a*) bulk ejection (stage 4.1) and (*b*) partial ejection (stage 4.2). As the engulfed water is accelerated during engulfment, a small amount of water may exit the mouth, but the bulk of the water is captured and rebounds back and forth within the buccal cavity. The solid black lines represent the long axis of the body and jaws. The solid red line denotes the expanding buccal cavity. The engulfed water is shown in blue and the directions of its movement are represented by black arrows.

Internal flows represent the water that is to be or is being engulfed by the whale. External flows characterize the fluid mass that is never to be engulfed and instead moves around the animal. Such a distinction brings in a crucial simplification, namely that of distinguishing between *engulfment drag* and *shape drag*. Conceptually, the former would reflect the effects of muscular actions on the engulfed mass that may take place within the buccal cavity. Shape drag, on the other hand, would be the force of water resistance that results from the trajectory of the external flow and of the pressure that they exert on the animal as a direct result of its motion. This contrasts with merging both engulfment drag and shape drag into a single drag force of the V^2 type, where V represents body speed, as done in a previous study (Goldbogen *et al.* 2007). Such an approach involves the use of a time-dependent drag

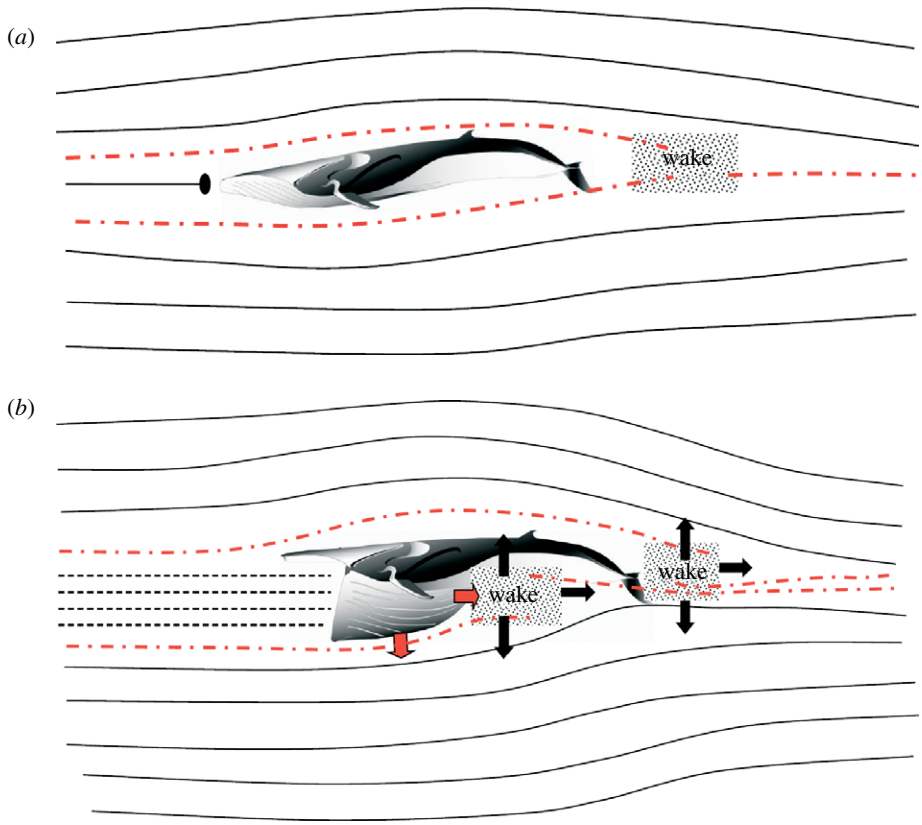

Figure 4. Simplified hydrodynamics about a large, rorqual-type whale during (*a*) a steady swimming and (*b*) a lunge at maximum gape angle. The solid black lines represent the streamlines of external flow whereas dashed black lines represent internal or engulfment flow. The streamline that ends with a circle shows the stagnation point. The thick red dashed lines correspond to near-boundary and wake flow. The red and black arrows indicate the general expansion during the lunge, of buccal cavity, mid-body near-wake and tail near-wake.

coefficient, which is usually obtained empirically. In a sense, the strategy adopted here actually yields a derivation of this coefficient.

Separating external and internal flows is obviously an approximation given the pliable nature of the buccal cavity, which, through its longitudinal and transverse expansions into the external flow, may transfer significant amounts of energy from one into the other as suggested in figure 4, and as is commonly seen during parachute inflation (Desabrais & Johari 2003). Here the BLFm takes advantage of the fact that muscle actions within the VGB may substantially stiffen the cavity wall, in a manner that minimizes the wall deformations into the external flow that would normally result from the excess internal flow momentum impacting the wall. As an added bonus, such extra stiffness might reduce the cavity expansion rates as well.

Using the decoupled, two-component drag idea means that the drag generated by the internal flow would be computed only from the prescribed buccal cavity wall forces pushing the engulfed water forward (figure 2). On the other hand, and as a result of additionally invoking negligible rates of external flow momenta being pushed *transversely* to the direction of the lunge, shape drag would be obtained from the type of *quasi-static* V^2-drag formula that is commonly used in biomechanics (Vogel 1994). Here, the associated drag coefficient would still be time dependent, but only in a manner that reflects the changing shape of the buccal cavity during engulfment, i.e. without any regard to the unsteady character of the transverse external flow that may exist. This restriction means that such drag coefficients would be those obtained from water tunnel drag studies performed at constant flow speeds, and with *solid* whale models of increasing cavity volumes and shapes as depicted in figures 1 and 5. (Note that these solid models would have to be attached to a cylinder sticking out and forward of the mouth, in order to mimic the external flow pattern shown in figure 4*b*.) In the absence of such supporting water tunnel data, however, the BLFm results discussed in §2.3 will use 'fitted' drag coefficient values, namely values yielding good trajectories in comparison with digital tag data.

2.3. One-dimensional hydrodynamics and buccal cavity shape

The engulfed mass shall be pictured as a long train of individual slugs of dimensions determined not only by mouth size, but also by the whale and reflux dynamics taking place at the time each is being engulfed (figures 2 and 5). Such a slug-tracking approach has been used with great success in the past, for example in parachute inflation simulations of the recontact of the wake onto a rapidly decelerating parachute (Spahr & Wolf 1981). In the BLFm, slug dynamics will be determined by the laws of one-dimensional hydrodynamics in which all the

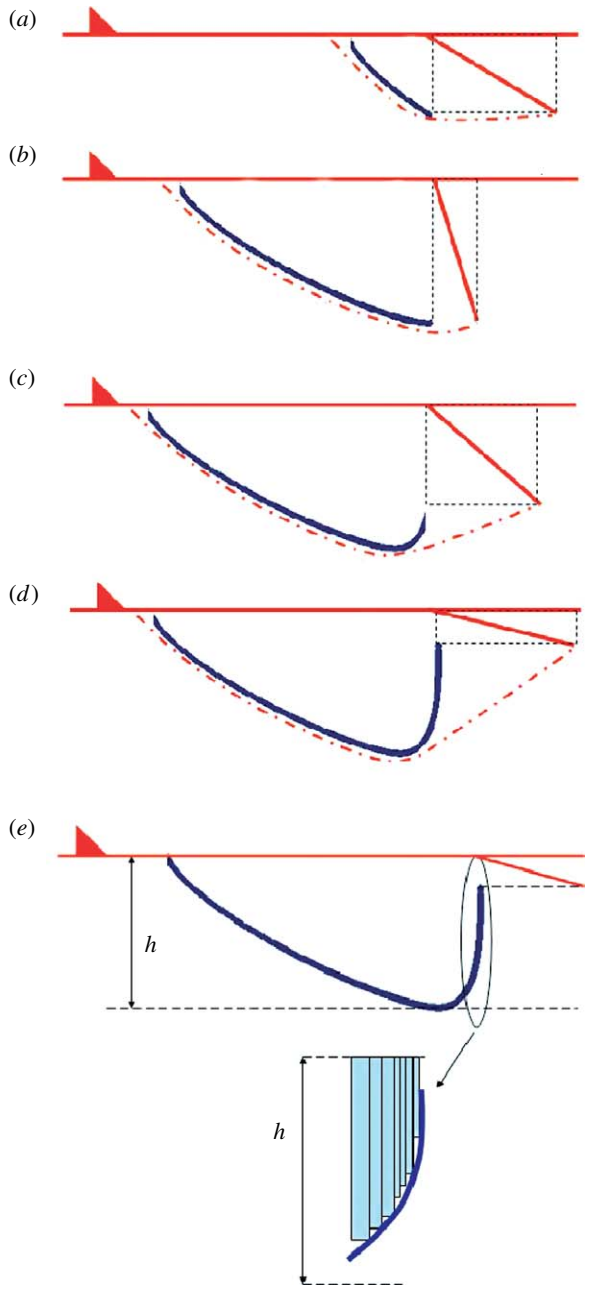

Figure 5. Buccal cavity expansion around engulfed water slugs. Outline of a typical simulated engulfed mass (thick blue curve) versus assumed belly outline (red dot-dashed line) during (*a*,*b*) mouth opening and (*c*,*d*) mouth closing. The belly outline is offset to show the difference between the two. The solid red lines represent the longitudinal axis of the body as well as dorsal fin, rostrum and mandible as in figure 3. The horizontal side of the dashed rectangles drawn from the mandible defines the horizontal projection of the belly outline anterior to the temporomandibular joint; their vertical side outlines the profile of the mouth area $A_c(t)$ at the temporomandibular joint. (*e*) Magnified view of the water slugs making up the engulfed mass towards the end of mouth closing.

relevant motions and forces evolve along only one dimension, namely that of the whale's longitudinal axis. This follows from the assumption that the energy and momentum being transmitted to the engulfed water (while inside the cavity) are used mostly to move it forward and longitudinally, rather than to change its shape or to impart transverse sloshing and/or turbulent motion. Video footage of a rorqual whale's underbelly during engulfment shows some evidence for sloshing (Bryde's whale *Balaenoptera edeni* lunges; BBC Blue Planet: Open Ocean Chapter), but such motions appear to be confined to small sizes relative to overall cavity radius, and occur mostly towards the end of mouth closure. In other words, one-dimensional unsteady hydrodynamics captures the physics most relevant to the whale's momentum changes and at the most important scale.

In mathematical terms, the explicit use of one-dimensional (and incompressible) hydrodynamics involves the use of equations expressed as functions of time and x, the latter being a spatial coordinate running along the longitudinal axis of the whale, for the calculation of the water velocity and pressure within the buccal cavity (see appendix A.4). Viscosity effects are altogether absent here given that flow shear is an inherently two- and three-dimensional phenomenon. We note that, in principle, an 'effective' one-dimensional model of viscous effects could be built, perhaps in a manner analogous to that of steady-state Poiseuille flow (Vogel 1994), but such a formalism may be quite complicated given the unsteady nature of the flow, and nonetheless expected to contribute only minimally given the large diameter-over-length ratio of the cavity. The main implication of the use of one-dimensional inviscid hydrodynamics here is that every portion of each engulfed water slug is moving in the same direction, as shown in figure 2, without the (small) eddies or curvilinear flows that are expected to be present.

The assumption of water incompressibility means also that all parts of each slug within the buccal cavity are moving at the same speed. In effect, the engulfed water behaves as a non-deformable solid, with a transverse shape defined by the mouth's cross section at the particular time that each slug enters the cavity. Each slug length is proportional to the slug's speed relative to the mouth at the time of engulfment. As an empirical input defined by the mouth outline at the temporomandibular joint (Lambertsen *et al.* 1995), the mouth cross-sectional area that is normal to the flow is controlled by changes in gape angle (Goldbogen *et al.* 2007). Thus, the faster the water enters the mouth, the longer the slug, and, similarly, the wider the mouth opening, the larger the cross section of each slug.

An example of the type of engulfed mass shaped from slug accumulation is shown in the magnified frame of figure 5*e*. In general, individual slugs are too narrow to be perceptible and therefore cannot be resolved in figure 5*a–d*, a result of their length being proportional to a time-scale interval of the order of 0.01 s. With slug length being intimately related to speed, the simulations presented here yield engulfed train lengths that are determined by the dynamics of the engulfment process, under the maximum constraint of the longitudinal length of the VGB. The shape of the engulfed water slugs remains the same through time, a concept that follows again from one-dimensional hydrodynamics where transverse fluid motions are largely absent.

Because dynamic pressure drives the expansion of the buccal cavity, the VGB is expected to adopt a shape that should be similar to that of the incoming slug train, at least posterior to the temporomandibular joint, as shown in figure 5. (The latter also coincides with the axial location of the cross-sectional area used in the calculation of the engulfed flux.) This portion of the buccal cavity is where the flow is constrained by soft tissue over all directions but one, and where ambient pressure is expected to be markedly different (and higher) from that of the surrounding water. On the other hand, the water within the mouth, i.e. anterior to the temporomandibular joint (inter-mandibular space), is not considered as being 'engulfed' by the BLFm, an assumption based on the fewer volumetric constraints that would allow flows across the mandibles in addition to flows towards the ventral cavity. The momentum gained by such flows (with respect to an initial state of rest) should be much smaller than that of the flows in the ventral cavity posterior to the temporomandibular joint. As a result, the outline of the ventral blubber anterior to the temporomandibular joint is arbitrarily made to follow a line that stretches from the tip of the mandibles to the point of maximum lateral expansion of the VGB (figure 5*c*,*d*).

Such assumed ventral shape is clearly an over-simplified view of the real shape but is made necessary to facilitate the computation of the length of the stretched VGB over time, as explained in further detail in appendix A.2. However, such a simplification should only be a minor problem since all the momentum and engulfed mass calculations in the BLFm are based on volumetric (i.e. bulk) properties of the engulfed mass rather than on the specific shape of the ventral blubber.

2.4. Buccal cavity wall forces during engulfment: anatomical considerations

Given the general state of ignorance on the specifics of the muscular action taking place inside the mouth, the engulfment modelling described herein incorporates the use of prescribed forces that are surmised by morphological data. With the complex muscle contractions that may or may not drive the engulfment process, such forces are expected to vary in both magnitude and duration over the course of a lunge. Thus, the BLFm has been designed to accommodate a wide variety of cavity wall forces, in order to yield either passive or active interactions of the VGB with the engulfed mass.

The VGB is composed of a series of longitudinal ridges separated by dense elastic tissue (Orton & Brodie 1987). Three muscle layers are closely associated with the blubber, with two outer layers oriented $\pm 45^{\circ}$ with respect to the third layer that runs longitudinally. Interestingly, such tissue arrangement yields stress–strain properties that make the buccal cavity wall a very inefficient device for the storage of elastic energy during the early and mid-portions of the engulfment process (Orton & Brodie 1987). Indeed, longitudinal stress shows almost no build-up until a strain of approximately 50 per cent is attained, at which time it increases exponentially (figure 6). The circumferential stress–strain curve, on the other hand, shows

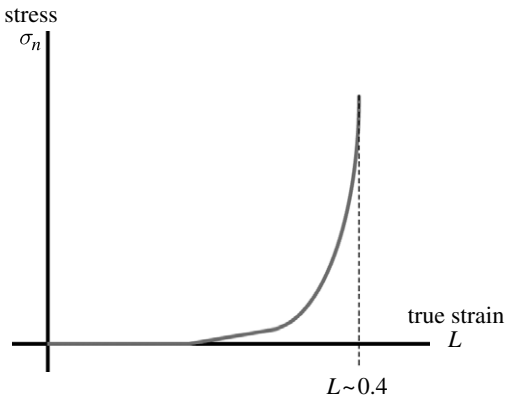

Figure 6. Schematic of the longitudinal stress–strain data compiled by Orton & Brodie (1987).

a somewhat greater elastic energy storage capacity, which is reached only during 130–270% strain, prior to an exponential increase in stress at 300 per cent strain. From these data, Orton & Brodie (1987) suggested that, during lunge-feeding, the engulfed water is not pushed forward nor moved backwards via suction, but rather enveloped with the compliant VGB. Under such conditions, little resistance is generated to the advance of internal flow unless active muscle contraction within the buccal cavity is involved. As will be shown here, pure 'compliant engulfment', i.e. engulfment without any throat wall push whatsoever, yields engulfment rates that are much larger than those suggested by the digital tags of real animals. Such evidence, together with the presence of well-developed muscle layers underlying the blubber, strongly suggests an active role played by the animal in regulating the flux of engulfed water via the application of throat wall forces with active muscle contraction. Such active regulation could be initiated consciously or unconsciously, unlike inflating parachutes where it is achieved passively via the tension build-up supported by the fabric, straps and suspension lines (Potvin 1999).

The very fact that engulfment may result from a series of coordinated muscular inputs for successful reflux management means that there will be many ways of achieving a successful lunge, of which only a few will be explored here. Not all possible muscle input profiles will be investigated in this paper, as they are probably too numerous and too complex for analysis in a first study (and, most probably, not all have yet been discovered). But the basic concepts and techniques discussed in §2.5 should be appropriate, not only for the future investigations of the case of depth-lunging explored in this paper, but also for the lunging performed either horizontally at the ocean's surface or vertically towards and through the surface. Obviously, the air boundary brings here a new constraint that will further limit the escape routes of the prey, thus changing the requirements for efficient reflux management and hence what constitutes coordinated muscle action. In the case of surface-breaking lunges, the possibility of pushing parts of the refluxed water *above* the surface also introduces even more constraints on how muscular inputs are to be metered out.

2.5. Prescribed buccal cavity wall forces

Our approach for defining the nature of the wall forces was inspired from physiology. In particular, we suggest that the types of buccal cavity wall force F_{BC} be specified by the purported information that a whale obtains during engulfment. Such information includes direct pressure sensing, given the presence of mechanoreceptors within the VGB (deBakker *et al.* 1997). These lamellated corpuscles are located medial to each groove and are present in both elastin and muscle layers, which are precisely those areas that are stretched during engulfment. Therefore, dynamic pressure during a lunge could be sensed at a single point inside the buccal cavity and reacted to with muscle activity. In this case, a buccal cavity wall force that is based on sensed dynamic pressure would be as follows:

$$F_{\mathrm{BC}}^{\mathrm{DP}}(t) = k_{\mathrm{DP}} \cdot A_{\mathrm{c}}(t)\left[\frac{1}{2}\rho_{\mathrm{w}}(V_{\mathrm{c}} - V_{\mathrm{w}})^2\right]. \tag{2.1}$$

Here, V_{c} and V_{w} correspond to the speed of the whale (or 'cetacean') and engulfed water, respectively, as measured from the shore. $A_{\mathrm{c}}(t)$ is the instantaneous cross-sectional mouth area measured below the temporomandibular joint (figure 5*e*), ρ_{w} is the density of salt water, and k_{DP} is a BLF-input 'reaction' constant used to simulate the degree to which the whale reacts to the sensed pressure (range $0 < k_{\mathrm{DP}} < 1$). The difference $V_{\mathrm{c}}(t) - V_{\mathrm{w}}(t)$ reflects the fact that the whale is sensing the pressure related to the flow relative to its body. The function $A_{\mathrm{c}}(t)$ is an empirical input derived from video footage and morphological data (Goldbogen *et al.* 2007), which for the 20 m adult fin whale considered here varies with time as follows:

$$A_{\mathrm{c}}(t) \sim 0.059t^4 - 0.729t^3 + 1.851t^2 + 2.321t. \tag{2.2}$$

Equation (2.2) entails that the cavity wall force developing in response to dynamic pressure will be greatest halfway through engulfment, i.e. when A_{c} is at its greatest and when $V_{\mathrm{c}}(t) - V_{\mathrm{w}}(t)$ is still large (e.g. when V_{w} is small and $V_{\mathrm{c}}(t) \sim V_{\mathrm{c}}(0)$).

We note that sensing dynamic pressure could also be involved during compliant engulfment, where the maximum dynamic pressure would be sensed (at $1/2\ \rho_{\mathrm{w}} V_{\mathrm{c}}^2$). In this case, the whale applies no resistance (i.e. no wall forces) to the advance of the water inside its cavity, and therefore the engulfed water should remain nearly stationary with respect to the shore (i.e. with $V_{\mathrm{w}} = 0$), or, in other words, be moving at V_{c} relative to the mouth. In the usual compliant engulfment scenario, the engulfed water would remain stationary until the water is purged out of the mouth. At this point, a significant wall force must be applied to accelerate the engulfed mass from a state of rest up to a speed that exceeds that of the whale at that time. The force required to do so would be very large, given the size of the engulfed mass relative to the body, estimated here at 40 000–60 000 kg with adult fin whales. Obviously, such a large force could be provided by the circumferential elastic stresses of the VGB (Orton & Brodie 1987). But given that purging is altogether left out in this current implementation of the BLFm, the buccal cavity wall force during compliant engulfment has a rather simple form, motivated in part by the elastic properties of the VGB that indicate very low stresses even at large strains, namely

$$F_{\mathrm{BC}}^{\mathrm{CE}}(t) = 0. \tag{2.3}$$

In contrast to sensing pressure at a single point, one could envisage sensing a pressure distribution over the entire buccal cavity in order to evaluate total engulfed mass. Sensing engulfed mass rather than flux (via dynamic pressure) should provide an altogether different kind of buccal cavity wall reaction, perhaps of the type illustrated by the following so-called 'shoving force' formulation:

$$F_{\mathrm{BC}}^{\mathrm{SH}}(t) = k_{\mathrm{S1}}\sqrt{\frac{2A_{\mathrm{c}}(t)}{\pi}}\frac{1}{\tau^2}M_{\mathrm{w}}(t), \tag{2.4}$$

with $M_{\mathrm{w}}(t)$ representing the total mass so far engulfed, calculated via the count of the number of slugs accumulating within the cavity, as explained in appendix A.1. The factor $\sqrt{A_{\mathrm{c}}(t)}$ represents a known relevant size scale (i.e. radius) for half-cylindrical mouth shapes, while the input constant τ corresponds to a time scale relevant to the dynamics of the shove. These are used together in the ratio $\sqrt{A_{\mathrm{c}}}/\tau^2$ to represent an acceleration scale relevant to how wall forces would be applied. In cases where the mouth is rather half-ellipsoidal (with constant skull width w), the shove-type force would instead have the following form:

$$F_{\mathrm{BC}}^{\mathrm{SH}}(t) = k_{\mathrm{S2}}\frac{4A_{\mathrm{c}}(t)}{\pi w}\frac{1}{\tau^2}M_{\mathrm{w}}(t). \tag{2.5}$$

The reaction constants k_{S1} and k_{S2}, similar to k_{DP} presented earlier, are non-dimensional inputs aimed at further fine-tuning the evolution of the muscular input. Note that the length scale τ can also change during the process, i.e. be smaller during mouth opening and larger during mouth closing, as will be shown in later simulations. However, given the temporal dependence of mouth area A_{c} and the fact that $M_{\mathrm{w}}(t)$ is monotonically increasing over the entire lunge, these wall forces would be maximum halfway through the lunge rather than at the beginning and/or end.

Interestingly, the shoving forces defined by (2.4) and (2.5) are analogous to those applied by the holder of a shovel in the process of collecting ice hockey pucks while skating. In cases where the skater is holding the shovel rigidly (with respect to the skater's body) and simply coasting (i.e. no skate stroking), a deceleration ensues with both skater and accumulated pucks moving at exactly the same velocities. Here, one has what is commonly known as completely inelastic collisions, where, in the case of a small puck collection rate, the shovel's force on the pucks is proportional to the total mass of pucks accumulated on the shovel and to the deceleration of the combined skater–(captured) puck body. Although such type of passive mass capture and shoving is commonly seen with swiftly inflating parachutes (Potvin 2008), it probably does not occur during lunge-feeding given that, here, the engulfed fluid virtually *never* moves at the same speed as the whale, even once inside the mouth, but rather with a speed

that is initially smaller (during stages 1–4.1) and then later on faster (stage 4.2). Instead, the relevant skater analogy suggests that the shovel motion is metered during the entire puck collection sequence, where a push forward is applied initially (with respect to the skater's body) and then gradually decreased moments later. Clearly, the process is 'active', i.e. depending on the exact manner in which the skater pushes the shovel. Thus, the shoving force is proportional to the engulfed mass, similar to the passive shoving force discussed previously, but proportional also to an (input) time-dependent acceleration scale that is different from the instantaneous deceleration of the whale.

Note that the buccal cavity wall forces described here are bulk-type forces, i.e. forces that result from the uniform push throughout the volume and surface of the engulfed slug train. This is an approximation, obviously, of a system in which it is more likely that the wall forces will vary over the surface of the cavity, axially as well as circumferentially. Also note that other easy-to-construct bulk-type wall forces are, of course, possible, no less those based on elastic-type forces, either linear (i.e. Hookian) or nonlinear. Such forces could be modelled by the *circumferential* stress–strain data of Orton *et al.* (Orton & Brodie 1987), and used towards the very end of mouth closure when the buccal cavity is circumferentially extended. Elastic forces could be very important throughout lunging in the case of juveniles undergoing significant morphological changes as they develop into lunge-feeding adults.

3. EQUATIONS OF MOTION AND OTHER APPLIED FORCES

3.1. Collision between water and whale

The BLFm calculates the trajectory of whale and engulfed water based on the Newtonian equations of motion for each body,

$$M_c a_c(t) = T(t) - F_{ED}(t) - F_{SD}(t) + F_{ext}, \quad (3.1)$$

$$M_w(t) a_w(t) + V_w(t)\rho_w A_c(t)[V_c(t) - V_w(t)] = F_{BC}(t) - F_{ww}(t). \quad (3.2)$$

Following the convention of equation (2.1), and as described further in appendix A.1, the pairs M_c and a_c, and a_w and $M_w(t)$, correspond to the mass and acceleration of an empty whale and engulfed water, respectively. We used the mass of an averaged adult fin whale (50 000 kg, 20 m body length) in order to correspond to the kinematic data collected from digital tags (Goldbogen *et al.* 2007). These accelerations are defined from the velocities $V_c(t)$ and $V_w(t)$ measured from a fixed reference frame, say, located on the shore (where $a_c = dV_c/dt$ and $a_w = dV_w/dt$). All the forces applied on each body appear on the right-hand side (r.h.s.) of these equations. These forces consist of (figure 2) the buccal cavity wall force (F_{BC}) previously discussed (equations (2.1) and (2.3)–(2.5)), which by virtue of Newton's third law of motion will be considered as equal in magnitude to engulfment drag (F_{ED}), the tail thrust force (T), the weight-subtracted buoyancy force (F_{ext}) and, finally, the shape drag force (F_{SD}). Both T and F_{SD} will be described momentarily. The drag sustained by the engulfed water re-exiting the cavity (during stage 4) while interacting with the rest of the ocean is represented by F_{ww}. The mass $M_w(t)$ of the engulfed water is calculated by the model, as explained in appendix A.1. Unlike the mass M_c of the 'empty' whale, M_w is changing in time and computed by summing the individual masses 'dM_w' of all the slugs that have entered up to time t, where $dM_w = \rho_w A_c(t)(V_c(t) - V_w(t))dt$ with dt as a simulation time-step interval. Finally, note that the second term on the l.h.s. of (3.2) represents an extra contribution to the momentum of the engulfed water owing to its changing mass over time, a corollary of the more fundamental definition of momentum change: $d(V_w M_w)/dt = M_w dV_w/dt + V_w dM_w/dt$ (with $dM_w/dt = \rho_w A_c(t)(V_c - V_w)$).

Note that (3.1) does not include the effects of the lift generated by the body, fluke and flippers. As recently discussed by Cooper *et al.* (2008), such forces are important in determining the animal's pitching motions. Being generally orthogonal to the motion of the lunge, the effects of these forces are left out in this first version of the BLFm.

We finally note that equations (3.1) and (3.2) apply only to stages 2–4.1. Simulations of stage 1, i.e. pre-engulfment acceleration, involve the use of equation (3.1) only with $F_{ED} = 0$. The simulation of the partial ejection stage (stage 4.2), on the other hand, involves modified versions of (3.1) and (3.2) instead, to account for the portion of the engulfed water that leaves the buccal cavity towards the end of engulfment (see equations (A 1) and (A 2)).

3.2. Weight-subtracted buoyancy and fluke thrust

Buoyancy is an important factor for the energy budget of a lunge. When killed, rorquals typically will sink, thereby suggesting negative buoyancy (Ford & Reeves 2008). This idea is supported by kinematic data from diving fin whales, which exhibit gliding on descent and steady swimming on ascent (Goldbogen *et al.* 2006). This force naturally reduces the amount of active fluking that is necessary to generate sufficient speed prior to mouth opening, which may explain why rorquals can glide during the descent phase of a lunge (Goldbogen *et al.* 2006).

In its current implementation, the BLFm uses a simple model where the weight-subtracted buoyant force is assumed to be constant (in time) and independent of depth in such cases where vertical lunges are being simulated. Its value is an input of the model and will be represented by F_{ext}.

The BLFm uses a rather simple approach to thrust, namely the use of explicitly stage-dependent values that are constant over specified intervals; for example, $T(t) = T_{open}$ during stage 2 (mouth opening) and $T(t) = T_{close}$ during stage 3 (mouth closing), with T_{open} and T_{close} being BLFm input parameters derived from kinematic data (Goldbogen *et al.* 2006). A more detailed implementation could, of course, be designed from the formalism of Bose *et al.* (Bose & Lien 1989).

3.3. Shape drag and total drag

The drag associated with the changing shape of a lunging whale (figure 1) and the external flows that result (figures 1 and 4) can be parametrized by the following generally valid formula:

$$F_{\mathrm{SD}}(t) \equiv C(t)S(t)\left(\frac{1}{2}\rho_{\mathrm{w}} V_{\mathrm{c}}^2(t)\right). \tag{3.3}$$

Here, the surface area $S(t)$, later to be connected with $A_{\mathrm{c}}(t)$, serves as the forward-projected reference area that is needed for the complete definition of the so-called drag function $C(t)$. The latter is a dimensionless and time-dependent function, which represents the combined effects of the accelerating and decelerating external flows around the whale, as well as the effects of wake growth and wake turbulence that are generated during the lunge. Such generic, time-dependent formulation has been used in many areas of unsteady aerodynamics, in particular in parachute aerodynamics (Iversen & Balent 1951; Cochran *et al.* 1991; Higuchi *et al.* 1996; Doherr 2003; Potvin *et al.* 2003). We note that equation (3.3) is an alternative to another well-known approach that tries to avoid use of the hard to predict $C(t)$, by explicitly expressing F_{SD} in terms of an added-mass acceleration term proportional to $a_{\mathrm{c}}\mathsf{V}_{\mathrm{wake}}$ (where $\mathsf{V}_{\mathrm{wake}}$ is the wake's volume), an added-mass expansion term proportional to $V_{\mathrm{c}}\mathrm{d}\mathsf{V}_{\mathrm{wake}}/\mathrm{d}t$ and a 'form'-drag term proportional to $A_{\mathrm{c}}(t)\,V_{\mathrm{c}}^2$. At a fundamental level, such added-mass formulation is no less dependent on empirical inputs as (3.3), given that these mass terms also involve time-dependent proportionality constants that must reflect the actual temporal characteristics of the flows at hand (Sarpkaya & Isaacson 1981; Sarpkaya 1991; Potvin 2008).

Typically, the values of $C(t)$ may be much greater than those values characterizing the constant-speed regimes of fixed shape bodies, such as whales engaged in non-feeding travel, but $C(t)$ may also be much smaller as well, for example in cases involving substantial decelerations that involve significant recontact of the wake flows produced moments earlier (Strickland & Macha 1990; Potvin *et al.* 2003). The BLFm shall use a simplified version of (3.3) in which the drag area $C(t)S(t)$ is a time-varying, but stepwise, function defined as follows:

$$C(t)S(t)|_{\text{stage 1}} = C_{\mathrm{D1}}A_{\mathrm{c1}}, \tag{3.4}$$

$$C(t)S(t)|_{\text{stage 2}} = C_{\mathrm{D2}}A_{\mathrm{c}}(t) + C_{\mathrm{D1}}A_{\mathrm{c1}}, \tag{3.5}$$

$$C(t)S(t)|_{\text{stage 3\&4}} = C_{\mathrm{D3\&4}}A_{\mathrm{c}}^{\max} + C_{\mathrm{D1}}A_{\mathrm{c1}}. \tag{3.6}$$

Equation (3.4) specifies the drag area experienced by a whale accelerating through the pre-engulfment stage. Cross-sectional area A_{c1} is an input constant of order of 7.0 m^2 to match the basic dimensions of adult fin whales (Goldbogen *et al.* 2007). The drag function C_{D1} reflects the value of the drag coefficient during this stage, here set at a constant value of approximately $C_{\mathrm{D1}}=0.05$. Although based on whale maximum cross-sectional area (i.e. approx. 7 m^2), this value is consistent with that of Bose *et al.* (Bose & Lien 1989), namely $C_{\mathrm{D}}=0.0026$, which is based on an adult whale total body surface area of 131 m^2. Such a value is a steady-state value, but should be considered as acceptable for the pre-engulfment acceleration profile at hand, given the high degree of streamlining of the body during that stage.

Equations (3.5) and (3.6) reflect the drag areas adopted during mouth opening (stage 2) and mouth closure (stages 3 and 4), where $A_{\mathrm{c}}^{\max}$ is the maximum mouth cross section attained by $A_{\mathrm{c}}(t)$ at the very end of the mouth opening stage (equation (2.2)). In many of the simulations described below, the functions C_{D2} and $C_{\mathrm{D3\&4}}$ will have constant values, namely $C_{\mathrm{D2}} \sim 0.9$ and $C_{\mathrm{D3\&4}} \sim 0.6$, which yielded the best match of the experimental data. Such values are somewhat larger than those expected for similar non-expanding shapes moving at constant speeds, being a reflection of the unsteady character of the shape drag force during the lunge. Such variations of the drag function $C(t)$ between stages 2 and 3–4 have a very coarse time dependence, but one that reflects overall decreases in drag coefficient caused by increased shape streamlining over time, particularly during mouth closure, as well as by the recontact of the wake during deceleration (Strickland & Macha 1990; Higuchi *et al.* 1996; Potvin *et al.* 2003). Note that a more accurate description would have involved an increasing C_{D2} over time to reflect the expansion of the buccal cavity during stage 3. Finally, note that during stage 4, the forward-projected reference area becomes a constant, because, during mouth closing, the maximum circumference of the buccal cavity no longer changes (figure 1).

The total drag generated by the lunging whale can be computed from F_{SD}, calculated via (3.3)–(3.6), and from F_{BC} ($F_{\mathrm{ED}}=F_{\mathrm{BC}}$) as calculated from (2.1)–(2.5) and (3.1). As argued previously, this is possible only if the coupling between the internal and external flows is minimal, in which case $F_{\mathrm{D}}^{\mathrm{total}} \sim F_{\mathrm{SD}} + F_{\mathrm{BC}}$. As a result, we can define a total (unsteady) drag function $C^{\mathrm{total}}(t)$ as follows:

$$C^{\mathrm{total}}(t)|_{\text{stage 2}} \equiv \frac{(F_{\mathrm{SD}}(t) + F_{\mathrm{ED}}(t))}{(A_{\mathrm{c}}(t) + A_{\mathrm{c1}})\left(\frac{1}{2}\rho_{\mathrm{w}} V_{\mathrm{c}}^2(t)\right)}, \tag{3.7}$$

$$C^{\mathrm{total}}(t)|_{\text{stage 3\&4}} \equiv \frac{(F_{\mathrm{SD}}(t) + F_{\mathrm{ED}}(t))}{(A_{\mathrm{c}}^{\max} + A_{\mathrm{c1}})\left(\frac{1}{2}\rho_{\mathrm{w}} V_{\mathrm{c}}^2(t)\right)}. \tag{3.8}$$

Thus, the BLFm provides an approach to the calculation of an observable that was, until now, only available empirically (Goldbogen *et al.* 2007).

3.4. Water-to-water drag

The last addition to the collection of applied forces involved in a lunge is the hydrodynamic force applied on the engulfed slugs that are in the process of re-exiting the mouth during mouth closure (stage 4). These forces arise from the interaction of those slugs with the rest of the ocean that surrounds the whale. The BLFm represents this interaction with the drag-like

force F_{ww} that appears in equation (3.2),

$$F_{ww}(t) = 0 \quad V_w \leq V_c, \tag{3.9}$$

$$F_{ww}(t) = C_{Dww} A_c(t) \left(\frac{1}{2} \rho_w V_w^2(t) \right) \quad V_w > V_c. \tag{3.10}$$

The constant C_{Dww} is another user-supplied input for which a value of approximately 0.1 has been used here. Such a value is rather tentative given the current absence of hard data on the effects of the mixing between these two flows.

3.5. Mouth area and buccal cavity dimensions

The calculation of the profile radius R of the buccal cavity (figure 5) involves the assumption of a specific shape of the expanded buccal cavity. The mouth cross-sectional area A_c is a known input to the model that is derived from morphological data (Goldbogen *et al.* 2007). However, knowledge of mouth area does not imply knowledge of buccal cavity shape or of its linear dimensions. To mimic the ventral shapes of real animals with some accuracy, we approximated the expanded buccal cavity as either a half-cylinder, where $A_c = (1/2)\pi R^2$, or a half-ellipsoid of width w (where $w = 2.2$ m; approximate skull width of an adult fin whale), where $A_c = (1/4)\pi wR$. Half-cylinders would appear to be in order during the early stages of mouth opening, as well as during the later stages of mouth closing, whereas half-ellipsoids would be more appropriate during maximum gape angles, when the mouth's shape closely follows the outlines of the jaw (itself a very pronounced half-ellipsoid). The overall shape is probably a complicated mix of these two shapes, and thus any calculations of the length of the projected ventral outline will have some error. However, the error will have minimal impact on the calculated dynamics given that the essential inputs do not include the knowledge of a specific shape but only of a specific area.

3.6. Pre-engulfment acceleration

The body acceleration that precedes engulfment is where the whale builds up the kinetic energy that will be used to partly power the engulfment stage. Simulating this stage is not as much for the study of whale drag, as it is for obtaining a good estimate of the energy spent by the whale in generating thrust during acceleration. The digital tag data (Goldbogen *et al.* 2006, 2007) show a whale typically accelerating, prior to mouth opening, while swimming downslope over a vertical distance of approximately 10 m and a horizontal distance of approximately 20 m, and over time intervals of approximately 10 s. Borrowing from such data, the BLFm simulation duration of this stage lasted 10 s. On the other hand, the trajectory, a downslope path, was simulated as a straight line (hypotenuse) angled by a height and run consistent with the data of the digital tags, namely 10 and 20 m, respectively. This allows the use of the one-dimensional model of equation (3.1), where the external forces $T + F_{ext}$ correspond to projection of the thrust, buoyant and weight forces along the path, namely $T + F_{ext} \rightarrow \text{thrust} - (\text{buoyancy} - \text{weight}) \times \sin(64°)$. As no data are currently available on the actual buoyancy and fluke thrust of the tagged whales, the input $T + F_{ext}$ was given values that allow the best match of the tag data. As mentioned previously, no water is being engulfed here, hence the input $F_{ED} = 0$. The last ingredients are the input parameters for the shape drag force (equations (3.3) and (3.4)), which, as discussed in §3.3, amount to $C_{D1} = 0.05$ and $A_{c1} = 7\ \text{m}^2$. The amount of work involved during pre-engulfment (as well as during engulfment) was calculated by the standard integration $\int F\, dx$ of the force F under consideration over distance travelled, where $dx = X_c(t + dt) - X_c(t)$.

4. SIMULATION PROCEDURE AND TERMINATION

4.1. BLFm simulation protocol

The solutions of the BLFm are obtained numerically via a time-based iterative scheme, where the values of a_c and a_w are calculated from equations (3.1) and (3.2) (and equations (A 1) and (A 2)) at each value of discretized time, namely at $t = dt$, $2dt$, $3dt$, etc., with the step size dt being a known input value that is much smaller than the duration of each of the four engulfment stages (typically of the order of 0.01 s). The computation is performed sequentially at each value of t, after having first performed the following tasks.

(i) Engulfment stage determination performed by monitoring the values of the mouth cross-sectional area A_c as per equation (2.2), which increases during mouth opening (stage 2) and decreases during mouth closing (stages 3 and 4); note that the pre-engulfment simulation is performed separately, i.e. in another simulation.
(ii) External force calculation of all the forces appearing in the r.h.s. of (3.1) and (3.2), as well as of the second term in the l.h.s. of (3.2).
(iii) Engulfed mass calculation of $M_w(t)$, which is the summation of the mass $\rho_w A_c(t)(V_c(t) - V_w(t))dt$ of each slug so far engulfed (see equation (A 3)).

Once the values of a_c and a_w are determined, they are used to update the speeds $V_c(t)$ and $V_w(t)$, as well as the positions $X_c(t)$ and $X_w(t)$, using well-known numerical analyses (see appendix A.1 for further details). Deciding whether the cavity forces under consideration correctly described the kinematics of a lunge was based on: (i) matching of digital tag data, and (ii) yielding a termination of engulfment that coincides with the time of complete mouth closure.

4.2. Simulation-stopping criteria: maximum inflation

The total length of the train of engulfed slugs is known at all times, being calculated by the function $X_c(t) - X_w(t)$ representing the separation between the temporomandibular joint and the leading engulfed slug ($X_c(t)$ and $X_w(t)$ are computed from the known velocities $V_c(t)$ and $V_w(t)$). A simulation stops whenever

$X_c(t) - X_w(t)$ is greater than the maximum longitudinal extension of the VGB L_{max}^{long} minus palatal length, which for the tagged adult fin whale under consideration (20 m body length) was measured at approximately 8 m (True 1904; see appendix A.2). Note that with such a stopping point, the engulfment process *may terminate prior to mouth closure*, depending on the specifics of the shape drag and engulfment drag forces being prescribed. Thus, the engulfment process can be terminated dynamically. Again, we note that all the forces at play (figure 2) must be applied in a well-coordinated manner for engulfment to terminate at the very moment of complete mouth closure.

4.3. Controlling the over-draining problem

By design, BLFm simulations can also terminate prematurely when the cavity *over-drains*, i.e. loses a water mass that is equal to or *greater* than the entire mass so far engulfed. Over-draining occurs when large-enough buccal cavity wall forces are exerted on small slugs of engulfed water, resulting not only in the rapid ejection of engulfed water but also in a negative value of the engulfed mass M_w (see appendix A.3). This condition arises from the mouth area (A_c) being, by definition, quite small at the very beginning of mouth opening, thereby yielding small engulfed masses at such times. Of course, over-draining does not occur in nature, as it would entail not only the complete loss of the engulfed mass but also of fluid (or tissue) that is part of the whale prior to a lunge. But premature draining, where only the engulfed mass is lost, could occur if the animal applies too large a force on the mass so far engulfed. Thus, cavity wall force management *is* a crucial issue early in the engulfment process, both numerically and in nature.

In mathematical terms, over-draining arises as follows. Analysis of equation (3.2) at times $t_1 = 0$ and $t_2 = 0 + dt$ reveals that the speed V_w of the engulfed water at time t_2 may exceed the value of V_c at both t_1 and t_2, thereby yielding a negative M_w whenever the following inequality applies:

$$F_{BC} > F_{BC}^{thres} \equiv \rho_w A_c(t_2)(V_c(t_1))^2. \tag{4.1}$$

Under dynamic pressure-based wall forces, whose magnitude is largely determined by k_{DP} (equation (2.1)), the engulfed mass speed at t_2 ($V_w(t_2)$) is related to F_{BC} as follows:

$$V_w(t_2) = \frac{F_{BC}(t_2)}{\rho_w A_c(t_2) V_c(t_1)}. \tag{4.2}$$

Integrating (2.1) into (4.2) yields $V_w(t_2) = V_c(t_1) k_{DP}/2$. The result means that to avoid over-draining, where $V_w(t_2) > V_c(t_1)$, the value of k_{DP} shall be bound to $k_{DP}/2 < 1$.

We note that over-draining could be avoided with the help of other forces, for example when a suction force is applied just prior to mouth opening, to allow a 'buffer' water mass to be engulfed and *then momentarily immobilized within the mouth*. Such a buffer mass being much larger than the usual engulfed mass at small times ($M_w(0) \gg dM_w = \rho_w A_c(0) V_c(0) dt$) could then be pushed forward at slow-enough speeds. Engulfment could then proceed by the application of dynamic pressure-based forces on that buffer mass. Applying such an over-draining-avoidance strategy to the type of dynamic pressure-based force defined by equation (2.1), the small time dynamics of the solution, and consequently the allowable values of k_{DP}, would take the following form:

$$V_w(t_2) \sim a_w(t_2) dt = \frac{F_{BC}(t_2)}{M_w(t_1)} dt \sim \frac{k_{DP} \frac{1}{2} \rho_w A_c (V_c(t_1))^2}{M_w(t_1)} dt. \tag{4.3}$$

This result is obtained from equations (3.2) and (2.1) at small values of time t (with assuming $V_w(t) \sim 0$). Here, $M_w(t_1)$ is no longer proportional to the infinitesimal dt but to a much larger value, i.e. that of the buffer. Thus, the avoidance of over-draining via the use of a k_{DP} value that is small enough to ensure $V_w(t_2) < V_c(t_1)$ would imply via equation (4.3) the following constraint: $k_{DP} < (2M_w(t_1))/(\rho_w A_c(t_2) V_c(t_2) dt)$. Interestingly, this result shows that at a fixed value of buffer mass, the value of k_{DP} becomes unbounded when repeat simulations are performed at ever smaller values of dt. In other words, the use of a buffer mass eliminates over-draining problems. Using the fact that the simulations discussed here are characterized by $dt = 0.01$ s, $A_c(t_2) = 0.02$ m^2 and $V_c(t_1) = 3$ m s^{-1}, one has $k_{DP} < (2\, M_w(t_1))/0.62$ kg. Perhaps the most interesting point of this discussion is the fact that the over-draining problem being present for both numerical and real whales motivates the retention of suction by lunge feeders well into adulthood.

The avoidance of over-draining during engulfment driven by mass-shoving forces also imposes constraints on the input reaction constants k_{S1} and k_{S2}. Integrating equations (2.4), (2.5) and (4.2) yields the following upper bounds if $V_w(t_2)$ were to remain smaller than $V_c(t_1)$:

$$\frac{k_{S1}}{\tau^2} < \frac{V_c(t_1)}{\sqrt{\frac{2}{\pi} A_c(t_2) dt}} \quad \text{(half-circular mouth area)}, \tag{4.4}$$

$$\frac{k_{S2}}{\tau^2} < \frac{\pi w V_c(t_1)}{4 A_c(t_2) dt} \quad \text{(half-ellipsoidal mouth area)}. \tag{4.5}$$

One notes the dependence of both r.h.s. on $1/dt$, which shows that, as preliminary simulations are repeated with smaller dt's, the upper bound increases to an infinite value as dt approaches a zero value. In other words, in a world where an exact solution could be found through analysis, constants k_{S1} and k_{S2} are unbounded. Therefore, shoved engulfment will not be afflicted by the over-draining problems encountered with the previous cases. With numerical solutions, on the other hand, dt is finite and will introduce over-draining solutions if dt becomes too large. In the simulations presented in §5.3, where $dt = 0.01$ s, $A_c(t_2) = 0.02$ m^2 (as per equation (2.2)) and $V_c(t_1) = 3$ m s^{-1}, the r.h.s. of (4.4) and (4.5) turn up as 2659 and 25 918 s^{-2}. These values are greater by four orders of magnitude than the values used here.

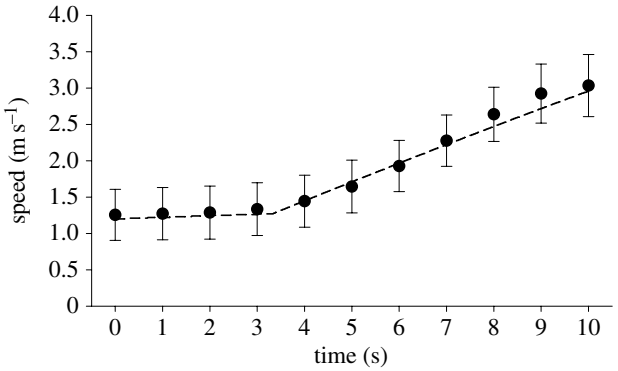

Figure 7. Velocity profile of an accelerating fin whale *Balaenoptera physalus* during the pre-engulfment phase. The average speed calculated from digital tags (Goldbogen *et al.* 2006, 2007) is represented by circles (error bars represent standard deviation). The dashed line represents whale speed predicted by the BLFm (computer run no. 0203).

5. RESULTS

The main results of the BLF simulations are shown in figures 7–12. All are based on a prototypical adult fin whale of 20 m body length with a 50 000 kg mass. As discussed previously, current morphological data obtained in the field imply a maximum longitudinal extension of the VGB of approximately 8 m past the temporomandibular joint, a palate length L_{palate} of approximately 4.1 m and a skull width w of approximately 2.2 m. Such a whale represents the group of individuals that were tagged in a previous study (Goldbogen *et al.* 2006) to produce the whale speed data also shown in those figures. These speeds were measured from the flow noise detected by a hydrophone located in the tag, thus yielding the smoothly varying data shown in the figures, averaged over a widely spread noise intensity scatter represented by the standard deviations also shown in the figures. We note that a direct comparison with speeds derived from accelerometers also mounted on the tag suggests those averages to become less accurate for speeds less than 0.5 m s^{-1} and exceeding 6 m s^{-1} (see Goldbogen *et al.* (2006, 2007) for further details).

5.1. Pre-engulfment simulation

Figure 7 shows the results of a simulation of the pre-engulfment stage, using the shape drag coefficient of $C_{\text{D1}}=0.05$ and surface area of 7 m^2 measured in other studies (§§3.3 and 3.6). The only *a priori* unknown parameter left here is the thrust–buoyancy coupling $T+F_{\text{ext}}$, which has been applied in the temporal stepwise manner, namely: $T+F_{\text{ext}}=0.10\times13\,500$ N for $0<t<3.33$ s and $T+F_{\text{ext}}=13\,500$ N for $3.33<t<10.0$ s. The initial speed was set at $V_{\text{c}}(0)=1.2$ m s^{-1} per digital tag data. The match appears quite good, although, perhaps, facilitated by the low temporal resolution of the experimental data (i.e. 1 Hz) and its significant scatter bounds.

It is interesting at this point to mention the energies associated with this case, a straightforward calculation from numerically integrating each force over the distance travelled. One obtains a 181 562 J gain of (whale) kinetic energy, caused by an input of 196 830 J contributed (mainly) by thrust and 14 424 J of drag loss. As shall be seen later, such energy expenditure during pre-engulfment forms a substantial part of the energy spent during an entire lunge.

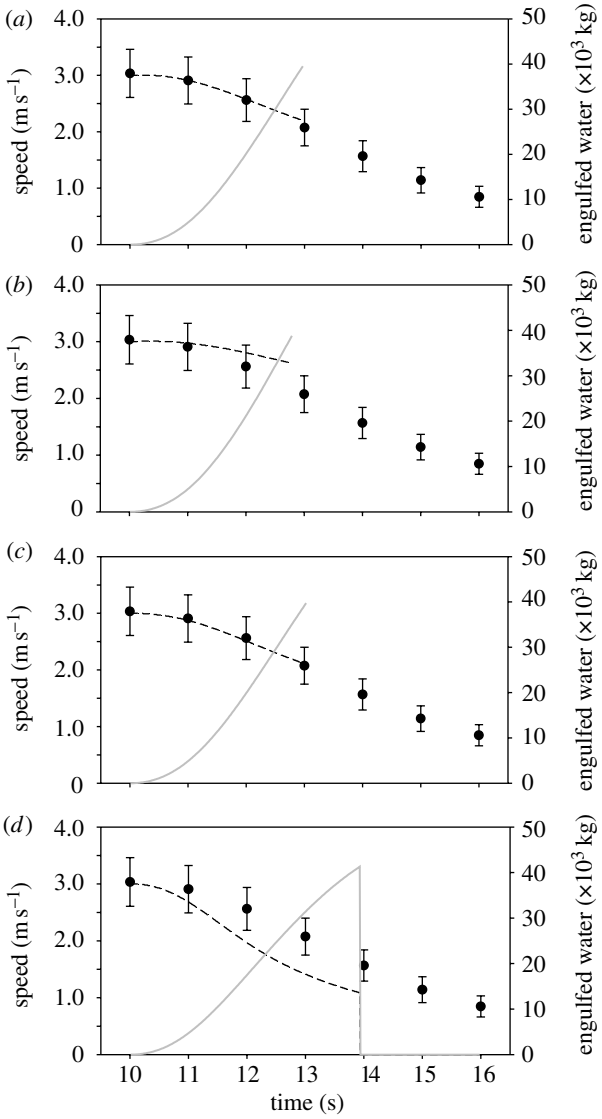

Figure 8. Whale speed and engulfed water mass during compliant engulfment. (*a*) Measured (black circles) and simulated (black dashed line; from runs (*a*) 1041, (*b*) 1060, (*c*) 1061 and (*d*) 2062) data of the whale during passive engulfment are shown as a function of time after mouth opening ($t=10$ s). The same simulation was repeated (*b*) with shape drag coefficients that have been decreased by half, where (*c*) $T-F_{\text{ext}}=0$ and (*d*) with extremely high shape drag coefficients=2.5. Each simulation terminates at $t\sim13$–14 s because maximum extension of the VGB occurs. The solid grey line corresponds to the computed engulfed mass.

5.2. Compliant engulfment

Compliant engulfment provides the simplest case to simulate, given that the absence of buccal cavity wall forces implies $F_{\text{BC}}=0$ (equation (2.3)). Here, shape drag provides the sole source of water resistance to the motion, with $C_{\text{D2}}\sim0.9$ and $C_{\text{D3\&4}}\sim0.6$ (§3.3). The parameter sum $T+F_{\text{ext}}$ is set at 2000 N (mouth

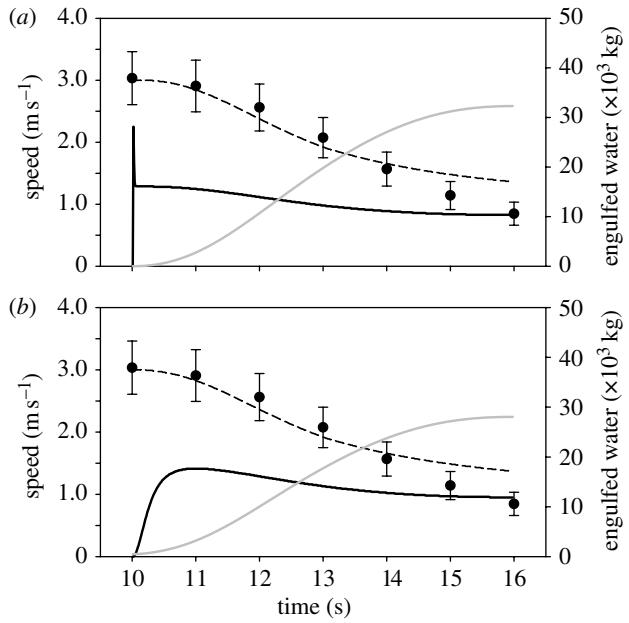

Figure 9. Dynamic pressure-dominated engulfment. The same representation as in figure 8 except that the solid black line represents the speed of the engulfed water. (*a*) Engulfment driven by dynamic pressure-based wall forces ($k_{DP}=1.5$) results in an incomplete filling of the buccal cavity and a rapid spike in engulfed water speed (computer run no. 1062). (*b*) Using suction to engulf a small buffer mass (500 kg) before force is applied ($k_{DP}=2.0$) removes the spike anomaly but incomplete filling still occurs (computer run no. 1066).

opening) and 0 N (mouth closing) to reflect the minor fluking seen on the tags. The results are shown in figure 8*a*.

Clearly, the absence of engulfment drag caused by zero-cavity wall push (figure 2) means that the engulfed water is not moving (relative to the shore); in other words, there is no reflux. Given the still-appreciable motion of the whale, one ends up with the rapid and premature filling of the buccal cavity. As discussed in §4.2, filling ends whenever the leading engulfed slug is reaching the umbilicus, after travelling a distance $X_c(t)-X_w(t)$ equal to approximately 8.0 m (as calculated from the difference $(L_{max}^{long}-L_{palate})$). Here, one sees clearly the VGB reaching full extension halfway through the lunge, i.e. to the end of stage 2 when the mouth is at maximum gape, rather than at the time of mouth closure.

Reaching fullness at the halfway point yields a velocity evolution that would be different from that displayed in figure 8*a* past the 13th second. By being at rest at $t=13$ s, all 40 000 kg of engulfed mass would now have to be set into motion *without any further travel past the umbilicus*. Even after allowing for a very small amount of extra stretching *per* the steep part of the Orton–Brodie stress–strain curve (figure 6), one has the general constraint $X_c(t)-X_w(t)\sim(L_{max}^{long}-L_{palate})$ (=const.), which means that the engulfed mass would now have to be accelerated to the speed of the whale, namely to $V_w(t)\sim V_c(t)\sim(50\,000/90\,000)\times 2\ \mathrm{m\,s^{-1}}\sim 1.1\ \mathrm{m\,s^{-1}}$, over a time interval that is much shorter than the 3 s that remains in the mouth closing stage. In other words, $V_c(t)$ would exhibit a steep change at about the 13 s mark, from $2\ \mathrm{m\,s^{-1}}$ to

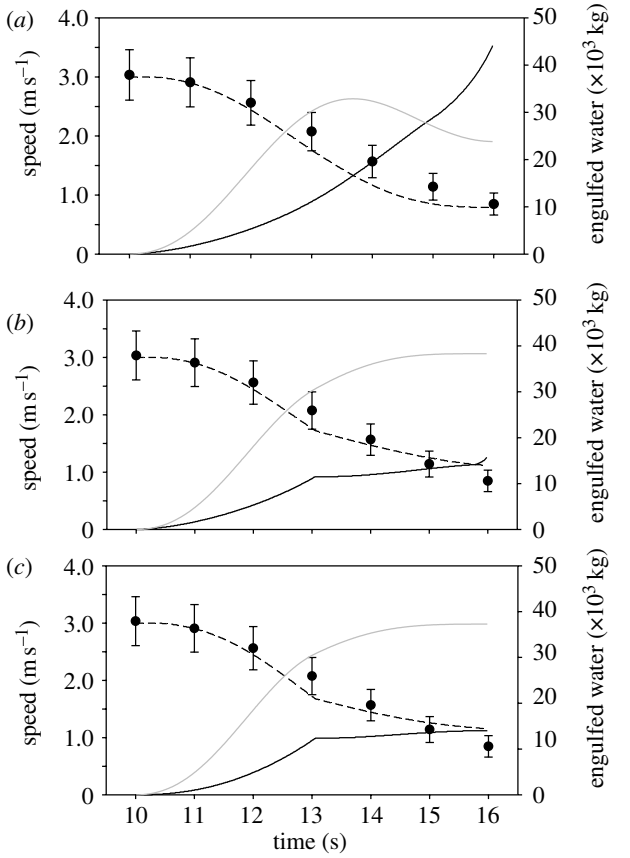

Figure 10. Shoving engulfment. (*a*) Simulation involving shove-type wall forces ($k_{S1}/\tau^2=0.34\ \mathrm{s^{-2}}$) and half-circular buccal cavity contour results in ejection of engulfed water (computer run no. 1064). (*b*) If shove forces are decreased halfway through the lunge ($k_{S1}/\tau^2=0.34\ \mathrm{s^{-2}}$ for $10<t<13$ s and $0.085\ \mathrm{s^{-2}}$ for $13<t<16$ s), complete filling occurs (computer run no. 1040). (*c*) Similar results are obtained when the overall shove force is decreased ($k_{S1}/\tau^2=0.18\ \mathrm{s^{-2}}$ for $10<t<13$ s and $0.036\ \mathrm{s^{-2}}$ for $13<t<16$ s) and half-ellipsoidal buccal cavity contour is used (computer run no. 1050).

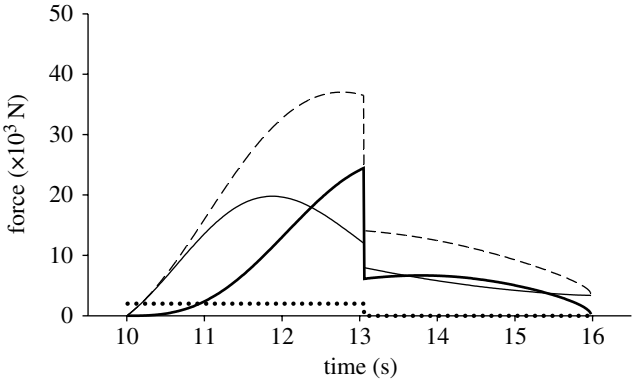

Figure 11. Forces produced during shoving engulfment (computer run no. 1040; figure 10*c*). Shove forces are applied during the first half of engulfment, as indicated by the thrust profile (dotted line). Total drag (dashed line) is the sum of external drag (thin solid line) and engulfment drag (thick solid line).

approximately $1.1\ \mathrm{m\,s^{-1}}$, a feature not seen in figure 8*a*. As will be seen with the other wall force examples, the smoothness of the digital tag data is more

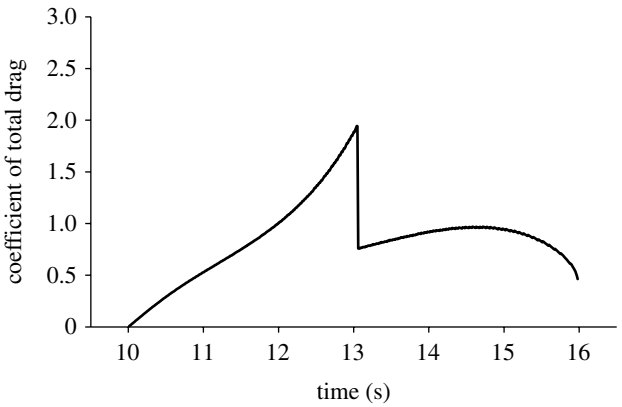

Figure 12. Total drag coefficient during shoving engulfment (computer run no. 1040). Total drag coefficient increases during the application of shove forces during mouth opening (figure 10*c*; $10<t<13$ s), and then rapidly decreases to initial values during mouth closure (figure 10*c*; $13<t<16$ s).

the result of a reflux that builds up from the very beginning of the lunge rather than from the halfway point, with the added benefit that the cavity filling rate is smaller by roughly a factor of 2.

It is interesting to note that despite the early filling of the buccal cavity, there is a good match between predicted and measured whale speeds during the first half of engulfment. When shape drag coefficients are decreased by half (with all other parameters unchanged), the buccal cavity fills even sooner, but again ends up with the predicted speed of the whale matching well with observed data (figure 8*b*).

Trying to synchronize cavity filling with the time of mouth closing by either reducing thrust or drastically increasing shape drag was unsuccessful, as shown in figure 8*c*,*d*. The trajectory shown in figure 8*c* corresponds to using zero propulsion in both stages, and figure 8*d* to shape drag being more than doubled, with $C_{D2}=C_{D3\&4}=2.5$ (in both cases, all other inputs are the same as those of figure 8*a*). We note that in figure 8*d*, which would correspond to an animal using the flippers as *hydro-brakes*, premature filling has been delayed by approximately 1 s, but at the cost of wasting 80 per cent of the (fluking) thrust energy that was spent during both pre-engulfment and engulfment. Further physical ramifications of these results will be discussed in §6.

5.3. Engulfment with constant wall forces

Using a constant wall force, where $F_{BC}\neq 0$, is a simple and obvious generalization of compliant engulfment, at least mathematically. This case also has pedagogical value as it exhibits several of the problems that may inhibit or accelerate engulfment.

Running the BLFm with a low value of F_{BC} over the entire engulfment process shows, again, the occurrence of premature buccal cavity inflation, with similarity to compliant engulfment. On the other hand, running at high-enough values of F_{BC} produces premature draining, as well as over-draining, as the result of very large buccal cavity wall forces being applied early on in stage 2 on engulfed slugs that are too small. In an example where $\mathrm{d}t=0.01$ s, $A_c(t_2)=0.02\ \mathrm{m}^2$ (as per equation (2.2)) and $V_c(t_1)=3\ \mathrm{m\,s^{-1}}$ (per digital tags), the r.h.s. of (4.1) yields $\rho_w A_c(t_2)(V_c(t_1))^2\sim 184$ N as the threshold beyond which over-draining always occurs, a very small (and unlikely) force indeed. This limit is a fundamental problem for the constant-force version of the BLFm, since at fixed F_{BC} and V_c, reducing the value of $\mathrm{d}t$ does not stabilize the simulation or improve convergence (as in most numerical problems), but, instead, continues to destabilize it further, as the value of $A_c(t_2)$ becomes even smaller. This numerical problem can be elegantly cured by the use of a little suction just prior to engulfment, as mentioned previously (§4.3) and further discussed in §5.4.

5.4. Dynamic pressure-dominated engulfment

In the case of dynamic pressure-based wall forces, the amount of push on the engulfed mass is regulated by the reaction constant k_{DP} (equation (2.1)). Here, simulations showed over-draining to occur whenever $k_{DP}>2$. Alternatively, a *minimum* value of k_{DP} ($k_{DP}^{min}\sim 1$) was evident, below which premature cavity filling once again takes place roughly at the mid-point of engulfment. This should not be surprising because $k_{DP}<1$ implies very small wall forces, which, with similarity to compliant engulfment, do not provide enough push on the engulfed mass to set it in motion and reduce the latter's high relative speed (i.e. relative to the mouth) into the cavity.

Having restricted the value of k_{DP} on physical grounds, a simulation with $k_{DP}=1.5$, $C_{D2}=0.9$ and $C_{D3\&4}=0.6$ (§3.3) was carried out to produce the results shown in figure 9*a*. Here, a poor match with experimental whale speeds near the end of engulfment ($15\ \mathrm{s}<t<16$ s) is evident, as well as incomplete buccal cavity inflation, with $X_c(t)-X_w(t)\sim 6$ m (rather than 8 m) by the time of mouth closure (at $t=16$ s). Several extra simulations have shown incomplete filling to occur over the entire permissible range of k_{DP} (i.e. $1.0<k_{DP}<2.0$). Interestingly, the only case where the cavity appears to fill completely occurs when $k_{DP}\sim 1.0$ with, however, a similar mismatch with the experimental data.

We note the presence of a significant and nearly constant reflux in the evolution of the engulfed mass speed $V_w(t)$, in contrast to compliant engulfment. We also note the discontinuity of the solution of figure 9*a*, for engulfed water speed V_w near $t=0$, from a zero value to approximately $V_w=1.3\ \mathrm{m\,s^{-1}}$ over an infinitesimal amount of time. Such a 'flaw' was observed during all simulations performed in the permissible range of k_{DP} as a result of $V_w(t_2)=V_c(t_1)k_{DP}/2$ being independent of the step size $\mathrm{d}t$ (see equation (4.2)). In other words, as extra simulations are repeated but with smaller and smaller $\mathrm{d}t$'s, the value of t_2 is reduced as well, but without the value of $V_w(t_2)$ ever changing as a result of $V_c(t_1)$ ($=V_c(0)$) being required to have the same value in all those simulations (i.e. $3.0\ \mathrm{m\,s^{-1}}$). This discontinuity can be cured by again resorting to pre-engulfment suction in order to secure a buffer mass (§4.3). Using, for example, a buffer mass of 500 kg along with $k_{DP}=2.0$ yields the curves of figure 9*b*, with a continuous engulfed slug speed evolution. However, the buccal

cavity fails to fill completely again and the mismatch with observed whale speed remains. Repeated simulations with lower buffer mass showed the same trend, but with $V_w(t)$ at small times ramping up more quickly, in a manner similar to what is seen in figure 9*a* (but without the spike). Additional simulations that involved higher k_{DP} (up to $k_{DP}=9$, buffer $=500$ kg) continued to show incomplete buccal cavity filling by the end of mouth closure.

5.5. Shoving engulfment

Engulfment lunges driven by mass-shoving forces of the type defined in (2.4) and (2.5) yield the trajectory evolutions of figure 10. Figure 10*a* is produced with $k_{S1}/\tau^2=0.34\ s^{-2}$, $C_{D2}=0.9$ and $C_{D3\&4}=0.6$ (§3.3), and with the same thrust profile used in the previous examples. The result is a poor match with observed whale speed at $14\ s<t<15\ s$. Most importantly, this run ends with the partial and unlikely ejection of 7000 kg of engulfed water during stage 3. On the other hand, a reaction constant reduced to $k_{S1}/\tau^2=0.085\ s^{-2}$ produces the premature filling of the cavity. Much better matches with experimental data are achieved when different values of k_{S1}/τ^2 are implemented during the mouth opening and closing phases, for example 0.34 and $0.085\ s^{-2}$, respectively, to reflect decreased muscular action at the end of the lunge. The results are shown in figure 10*b*, a case that also involves timely and complete buccal cavity filling. Interestingly, the small upward 'hook' appearing near the 16 s mark of the engulfed mass speed betrays the occurrence of the *partial ejection* stage depicted in figure 3*b*. Here, the sudden high acceleration is the result of only a small portion of the slug train being pushed out of the mouth. Similar results were also obtained with a half-ellipsoidal buccal cavity shape and smaller shove forces (stage 2, $k_{S2}/\tau^2=0.18\ s^{-2}$; stages 3 and 4, $k_{S2}/\tau^2=0.036\ s^{-2}$), hinting at the insensitivity of the overall kinetics with respect to ventral shape (figure 10*c*). Of note in both cases is the slow build-up of the reflux, to an endpoint of approximately $1\ m\ s^{-1}$. Such time-modulated uses of the shoving force represent so far the best prescription of wall forces matching tag data and yielding reflux moving nearly at the speed of the whale at the end of mouth closure.

Figure 11 shows the forces involved in the production of the trajectories highlighted in figure 10*b*. Figure 12 shows the corresponding evolution of the total drag function (see equations (3.7) and (3.8)). Despite the rapid decrease in shove halfway through the lunge, both shape and engulfment drag forces are comparable in magnitude during the entire simulation (figure 11). The coefficient of total drag shows a steady increase up until maximum gape ($C^{total}(t)=2.0$ at $t=13$), followed by a rapid drop back down to its initial value (figure 12). The mean coefficient of total drag during the entire inflation phase was at approximately 1.0.

Another interesting calculation enabled by the BLFm is that of the pressure gradient inside the buccal cavity. As shown in appendix A.4, the internal pressure difference $\Delta P(x, t)$ between two points separated by a distance x along the animal's longitudinal axis can be calculated exactly as $\Delta P(x, t)=\rho_w x \mathrm{d}V_w/\mathrm{d}t$. This, in turn, yields the pressure gradient $\Delta P/(X_c-X_w)$ over a distance separating the leading engulfed slug and the mandibular joint, being given by $\Delta P/(X_c-X_w)=\rho_w x \mathrm{d}V_w/\mathrm{d}t$. Such a gradient is an interesting estimate of the kind of pressure distribution that is to be expected inside the buccal cavity, which, in the case at hand, yields approximately $250\ Pa\ m^{-1}$.

The energy budget of the whale simulated in figure 10*b* is as follows: by the end of mouth closing, the total energy lost via shape drag and spent into the pushing of the engulfed mass amounted to 211 500 J, while the muscular energy spent as thrust totalled 15 750 J. Such numbers can be compared with the whale's kinetic energy just prior to engulfment, namely 225 000 J, generated, as we have seen, during the pre-engulfment stage. Adding the muscular energies invested during both pre-engulfment and engulfment yields a total expenditure of 298 080 J. This is a small expenditure of energy, assuming similar costs during the purging phase, compared with that gained by the processing of a typical catch of krill during a lunge (11 kg), which would yield approximately 40 000 000 J.

6. DISCUSSION

This study is the first attempt to model the unsteady hydrodynamics of rorqual lunge-feeding. A recent quasi-steady analysis of lunge-feeding predicted that an adult fin whale engulfs approximately $70\ m^3$, a volume of water that is greater than the volume of its own body (Goldbogen *et al.* 2007). However, those authors assumed a compliant engulfment mechanism where the VGB passively expands under dynamic pressure. Here, we show that such a mechanism is not plausible, at least when applied to the average adult fin whales tagged in a previous study (Goldbogen *et al.* 2006), as the VGB becomes fully extended much sooner, namely halfway through the lunge (figure 8). Such fast filling would entail rapid acceleration of a very large engulfed mass, over time scales of a second or less. Very large buccal wall forces would be needed for this, much larger in fact than those caused by shoving or by any other gradually metered muscle actions.

Interestingly, further compliant engulfment simulations have shown fillings to occur by the time of mouth closure *only for much larger whales*, i.e. for individuals characterized by $L_{max}^{long}-L_{palate}=13$ m. Such dimensions are attained when the separation between the tip of the lower jaw and navel has reached a length of approximately $L_{max}^{long}=20.5$ m (with a palatal length of $L_{palate}=6.6$ m), which according to fin whale morphological data (True 1904) would correspond to an overall body length exceeding 30 m. Fin whales, and even blue whales, do not exhibit bodies of such length (Lockyer 1976), and therefore this suggests that *pure* compliant engulfment may not occur even in the largest rorquals. However, it has to be pointed out that simulations for these 'large' whales were performed at the same mass (i.e. $M_c=50\,000$ kg), and with a cross-sectional area function A_c still given by equation (2.2). By not modifying A_c according to the size increase

under consideration, one is merely simulating a partial lunge, i.e. one performed with a maximum gape angle much smaller than 80°–90°. To simulate the full gape case would require A_c to increase at least linearly with overall body length with half-ellipsoidal cavities, or quadratically with half-circular cavities. With both cavity shapes, scaled area functions become larger than that of equation (2.2), a feature that would entail greater engulfment fluxes and, along with the required increased body mass, the possible return of the premature filling problem. This issue, together with others related to the scaling of initial lunge speeds, shall be further discussed in an upcoming publication. Finally, it should be pointed out that these simulations do not completely eliminate compliant engulfment even in adult fin whales. Lunges involving the *partial*, as well as quick, opening and closing of the mouth could define the conditions where it becomes a more energetically favourable strategy, particularly if the engulfed water is set into motion via rebound facilitated by elastic extension of the VGB.

Our simulations of active engulfment, where the whale develops muscle force to push engulfed water forward, resulted in complete filling only under certain conditions. In the case of a constant buccal cavity wall force, the water that enters the mouth right after opening is rapidly ejected owing to large forces being applied to small parcels of water. This is what happens, for example, when a solid and non-porous container is rapidly accelerated underwater: here, the increasing internal water pressure that builds up anterior to the container is rapid enough to prevent anything from being captured (Pivorunas 1979). Such draining and over-draining problems are also encountered with dynamic pressure-controlled wall forces, but can be avoided by the acquisition of a small buffer mass of water via suction, perhaps just prior to mouth opening. All whales presumably exhibit suction as neonates, and, as adults, rorquals are thought to depress their tongue to initiate distension of the buccal cavity during lunge-feeding (Lambertsen 1983).

On the other hand, the simulations have shown premature cavity filling not to be exclusive to compliant engulfment. This has been shown in the case of constant wall force strengths that were small enough to avoid over-draining. This points to another interesting observation concerning the value of the smallest force F_{BC}^{min} that is morphologically possible: here, the range of acceptable wall forces available to initiate engulfment without excessive premature emptying of the cavity could be estimated, in the absence of a buffer mass, by $F_{BC}^{min} < F_{BC} < \rho_w A_c(t_2)(V_c(t_1))^2$. Such a range increases with initial speed, but the energy cost associated with achieving it during pre-engulfment increases as well. These findings also point to a minimal initial speed needed to initiate engulfment without encumbering excessive and premature emptying of the cavity, of the order of $V_c(0) \sim (F_{BC}^{min}/(\rho_w A_c(t_2)))^{1/2}$. Interestingly, this speed could be similar across rorqual species of different sizes that scale according to geometric similarity, which, in turn, implies proportionality in F_{BC}^{min}.

Wall forces based on shoving, i.e. proportional to the so far engulfed water mass, provided the whale speed profiles that most closely match experimental data. The specific development of those forces and associated total drag coefficient are shown in figures 11 and 12. Maximum and average drag coefficient values during shoving engulfment are similar to those of swiftly opening parachutes (Potvin 2008), as well as quasi-steady calculations of lunge-feeding fin whales (Goldbogen *et al.* 2007).

Regardless of the type of lunge-feeding mechanism invoked, we found a good match between the predicted and observed whale speeds during mouth opening (figures 8–10). These results demonstrate the dominance of shape drag during the first half of engulfment (stage 2), where external flows primarily contribute to whale deceleration. On the other hand, the second half of engulfment (stages 3 and 4) is largely determined by the nature of active engulfment and the magnitude of buccal cavity wall forces applied to internal flows. In this way, internal flows are managed in order to successfully complete a lunge and avoid excessive buccal cavity wall forces.

It should be noted again that the specific evolutions of the reflux and whale deceleration shown in figure 10 can be achieved by cavity forces profiles other than discussed here. A sufficient condition for this may be for F_{BC} to gradually peak at about the beginning of mouth closing in the manner similar to figure 11. However, what remains clear is that, regardless of the specificities surrounding the form of F_{BC}, reflux will ensue and do so with the same biological consequences discussed here.

Active flow control via reflux probably contributes to maximum efficiency of the lunge-feeding process, enabling rorquals to execute as many lunges as possible during a dive. The cost of a lunge appears to be determined largely by the acceleration phase leading up the mouth opening. Such a characteristic will have a significant effect on the scaling of lunge-feeding performance and associated energetic costs. However, a rorqual probably has the ability to control other factors that drive lunge-feeding behaviour, such as maximum lunge speed and maximum gape angle. Future studies are already underway to determine the effects of these parameters on lunge-feeding performance and how different engulfment strategies might be more efficient for different-sized rorquals.

7. CONCLUSIONS

The advent of digital tagging to collect whale kinematic data in the field, together with the construction of models such as the BLFm, should open a new exciting chapter in the field of whale biology. Such experimental data provide the foundation upon which practical models can now be built to uncover previously unknown mechanisms and ideas. Here, we have shown how complex the physics of engulfment can be, with the introduction of new concepts such as active shoving wall forces, engulfed mass reflux, over-draining and buffer mass acquired via suction. More experimental and theoretical investigations are, of course, needed to elucidate the many uncertainties and approximations

that have been used here. On the theoretical side, the contributions of the VGB elastic properties as well as specific suction mechanisms for the generation of buffer masses (when needed) are being planned for addition into the BLFm. The involvement of the lift produced by the flippers and body will be considered as well.

Most importantly, the BLFm has to be further developed in order to simulate the lunge of any adult rorqual involving body dimensions and initial speeds other than those used here. Such development is needed to clarify the size and $V_c(0)$ dependence of the new constants and functions introduced in this study, for example k_{S2}, τ and $A_c(t)$, which were constrained by specific experimental data related to a representative ('average') adult fin whale. Only then will the BLFm provide the predictive framework needed to examine the scaling and physical limitations of lunge-feeding performance among rorqual species. This we hope shall be demonstrated very soon in an upcoming publication.

Funding was provided by NSERC to R.E.S. and a University Graduate Fellowship to J.A.G. J.P. would like to thank Saint Louis University and the University of British Columbia for the financial support provided to him for the completion of this study.

APPENDIX A. MATHEMATICAL DETAILS

A.1. Equations of motion

The calculation of whale and engulfed water speeds $V_c(t)$ and $V_w(t)$ is obtained from (3.1) and (3.2) during stages 1–4.1, and from the following coupled equations for stage 4.2:

$$[M_c + M_{meter}(t) - \rho_w A_c(t)(X_c - X_w)]\cdot a_c(t) = T(t) - F_{ED}(t) - F_{SD}(t) + F_{ext}, \quad \text{(A 1)}$$

$$[\rho_w A_c(t)(X_c - X_w)]\cdot a_w(t) + V_w(t)\rho_w A_c(t)[V_c(t) - V_w(t)] = F_{BC}(t) - F_{ww}(t). \quad \text{(A 2)}$$

The equations are used first to compute the accelerations $a_c(t)$ and $a_w(t)$. This is followed by the computation of V_c via the finite-difference version of $a_c \equiv dV_c/dt$ (Gould & Tobochnik 1996), and by that of the coordinate $X_c(t)$, via $V_c \equiv dX_c/dt$. This coordinate is defined as the distance between a point at the mandibular joint and the same reference point on the shore that was used to define $V_c(t)$ (figure 13). Computations of V_w and X_w are done similarly, with $X_w(t)$ being the distance between the leading edge of the very first slug engulfed (also herein referred to as the 'leading slug') and the same shore reference that defines $X_c(t)$. On the other hand, the function M_{meter} is the *water meter equation*, which tracks the amount of water being engulfed, namely

$$M_{meter}(t) \equiv \rho_w \int_0^t dt' A_c(t')[V_c(t') - V_w(t')]. \quad \text{(A 3)}$$

In equations (3.1) and (3.2) (i.e. during stages 2–4.1), one has $M_w(t) = M_{meter}(t)$. Because, during stage 4.2, parts of the engulfed water may be re-exiting the mouth, equations (A 1) and (A 2) involve the sum $(M_{meter} - \rho_w A_c(t)(X_c - X_w))$ to represent the mass of the engulfed water that now decelerates along with the animal, and $\rho_w A_c(t)(X_c - X_w)$ to represent the mass of the engulfed water that moves on its own according to the net external force exerted on it. In this model, the transition from stages 4.1 to 4.2 occurs when the following milestones are reached: (i) the mouth is closing, (ii) $V_w(t) > V_c(t)$, and (iii) $A_c(t) > 0.40 A_c^{max}$. Here, A_c^{max} is the maximum value of the open cross-sectional frontal area of the mouth being reached by the function defined in equation (2.2).

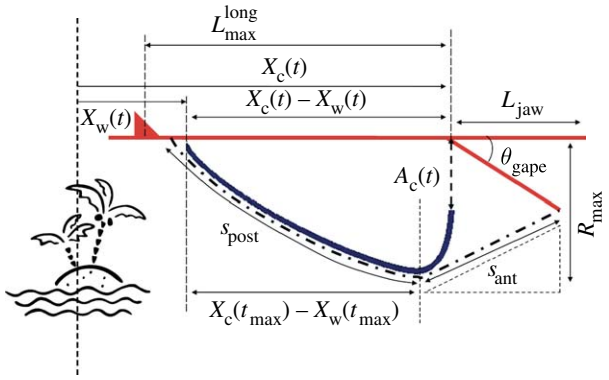

Figure 13. Basic definitions of the dynamical variables used in the BLFm, in particular equations (3.1), (3.2) and (A 1)–(A 4). The solid red lines represent the longitudinal axis of the body as well as the rostrum and the mandible as in figures 3 and 5. The shore-based reference frame is shown on the left. All other symbols and variables are defined in the text.

The simulations shown in figures 7–12 were obtained from the numerical integration of the equations of motion (3.1), (3.2), (A 1) and (A 2), using the simple Euler–Cromer algorithm (Gould & Tobochnik 1996). Although usually unsuitable for most multi-temporal scale simulations, Euler's method is accurate with the problem at hand, given that the two time scales operating here, namely that of the mouth cross-sectional area $A_c(t)$ and that of shape drag, are of the same order of magnitude, i.e. 10^0–10^1 s. As defined by equation (2.2), the changes related to $A_c(t)$ are of equal duration during both mouth opening and closing stages (3 s). The basic time scale of shape drag, on the other hand, can be estimated from the ratio $\tau_{drag} \sim M_c/(\rho_w V_c(0)\, SC_D)$ (derived from the integration of $M_c dV_c/dt = -(1/2)\rho_w SC_D V_c(t)^2$ with constant SC_D). Using $M_c = 50\,000$ kg, $SC_D \sim 1.0 A_c^{max} = 1.0 \times 8.7$ and $V_c(0) \sim 3$ m s^{-1} yields $\tau_{drag} \sim 2$ s. A check of the simulations, which were typically integrated using a time step $dt = 0.01$ s, was performed at a shorter time increment ($dt = 0.001$ s) and compared with those performed at the usual time steps. Such comparisons revealed no substantial differences in computed trajectories.

A.2. Slug and buccal cavity dimensions; simulation-stopping criterion 1

A BLFm simulation will track the physical dimensions of the engulfed slug train, thus enabling a calculation of the length $L^{ventral}(t)$ of the contour of the extended

buccal cavity. This step is based on the cavity shape defined in figures 5 and 13 (see also §3.5),

$$\left.\begin{aligned} L^{\text{ventral}}(t) &= s_{\text{post}} + s_{\text{ant}} \\ &= \int_0^{t_{\max}} \mathrm{d}t' \sqrt{\left(\frac{\mathrm{d}R}{\mathrm{d}t}|_{t=t'}\right)^2 + (V_{\text{c}}(t') - V_{\text{w}}(t'))^2} \\ &\quad + \sqrt{D^2 + H^2} \quad t > t_{\max} \\ H &= R_{\max} - L_{\text{jaw}} \sin\theta_{\text{gape}}(t) \\ D &= (X_{\text{c}}(t) - X_{\text{w}}(t)) - (X_{\text{c}}(t_{\max}) - X_{\text{w}}(t_{\max})) \\ &\quad + L_{\text{jaw}} \cos\theta_{\text{gape}}(t). \end{aligned}\right\} \tag{A 4}$$

The integral term measures the total ventral outline length (s_{post}) of the engulfed slugs up to the point of maximum slug area (generated earlier at the time of maximum mouth opening), while the second term in D^2 and H^2 (s_{ant} in figure 13) corresponds to the diagonal line outlining the presumed stretched skin running from the maximum mouth opening point to the mandibles. Here, the time $t_{\max}$ is the time at which the mouth stops opening and starts closing, thereby defining, according to equation (2.2), the moment of maximum cavity and engulfed mass projected radius $R_{\max}$. The calculation of $L^{\text{ventral}}(t)$ during the mouth opening stage proceeds similarly, but without the H term in s_{ant} and with $D = L_{\text{jaw}} \cos\theta_{\text{gape}}(t)$, as can be readily seen in figure 5.

Recalling §3.5, the value of $\mathrm{d}R/\mathrm{d}t$ and $R_{\max}$ will depend on the specifics of the assumed cavity shape, for example $A_{\text{c}} = (1/2)\pi R^2$ (half-circular mouth) or $A_{\text{c}} = (1/4)\pi wR$ (half-spheroidal mouth, with $w = 2.2$ m as a typical head width). The parameter L_{jaw} is another BLFm input that measures the longitudinal length between the tip of the rostrum and the midpoint, where the mandibles articulate with the base of the skull. Most importantly, equation (A 4) depends on the specific evolution of the gape angle θ_{gape} sustained by the mandibles. Fortunately, θ_{gape} is a known function that can be obtained from field data (Goldbogen *et al.* 2007),

$$\theta_{\text{gape}}(t) = (0.9668t^4 - 11.758t^3 + 36.219t^2 - 12.8724t + 0.0069)(\pi/180). \tag{A 5}$$

Note that a useful constraint on the value calculated by (A 4) is the value $L^{\text{ventral}}_{\max}$ of the maximum ventral outline length achievable, which could be independently obtained on dead specimen via the measurement of its maximum extended compliant length. Interestingly, the data of Orton & Brodie (1987) suggest $L^{\text{ventral}}_{\max} \sim 1.5 L^{\text{long}}_{\max}$ in cases where the *unextended* ventral blubber has a length similar to $L^{\text{long}}_{\max}$. The factor '1.5' arises here from the limit implied by longitudinal stress–strain data of Orton and Brodie, collected on adult dead tissue, showing no possible skin extension beyond 40–50 per cent of the unextended length (Orton & Brodie 1987; figure 6). In cases where the unextended ventral outline ($L^{\text{unextended}}_{\text{ventral}}$) is longer than $L^{\text{long}}_{\max}$, one should expect, instead, $L^{\text{ventral}}_{\max} = 1.5 L^{\text{unextended}}_{\text{ventral}} > 1.5 L^{\text{long}}_{\max}$. The fact that $L^{\text{unextended}}_{\text{ventral}} > L^{\text{ventral}}_{\max}$ has been documented before, for example in some film evidence (BBC Blue Planet) showing pronounced depressions of the VGB in between the mandibles during the initial stages of mouth opening. Also, post-mortem specimens show significant distension of the VGB (Gaskin 1982), suggesting that muscle contraction is required to hold the blubber close to the body and maintain a hydrodynamic shape when not feeding.

We note that using the maximum longitudinal extension length $L^{\text{long}}_{\max}$ as a signal for the ending of engulfment could be the wrong criterion in cases where significant circumferential expansion continues past the time of maximum longitudinal extension. This could be expected, for example, with animals featuring unextended ventral blubber that are significantly longer than $L^{\text{long}}_{\max}$, or with animals that could allow, via muscle relaxation, complete circumferential unfolding of the ventral furrows. Not only would such cases involve longer engulfment time, but they would also permit significant two- and three-dimensional flows for which the BLFm is no longer applicable.

Finally, it should be mentioned that the constraint $L^{\text{ventral}}_{\max} \sim 1.5 L^{\text{long}}_{\max}$ may or may not be applicable to juveniles, depending on the mechanical properties of the VGB and associated muscle layer.

A.3. Over-draining avoidance

As discussed in appendix A.2, the BLFm will yield unphysical answers in the form of a negative engulfed mass $M_{\text{w}}(t)$, when the wall force is large enough to expel all the slugs previously engulfed during the early times of the mouth opening stage. One way to avoid such a condition is to tune these forces to values that never cause V_{w} to exceed V_{c} at such times. This can be done by considering the basic equation of motion of the engulfed mass, namely equation (3.2), at the second time step of a numerical integration. After taking advantage of the fact that $V_{\text{w}}(0) = 0$, this equation becomes

$$M_{\text{w}}(0 + \mathrm{d}t)\, a_{\text{w}}(0 + \mathrm{d}t) \approx F_{\text{BC}}. \tag{A 6}$$

Using the meter equation (A 3) to estimate the engulfed mass at $t = 0 + \mathrm{d}t$ yields

$$M_{\text{w}}(0 + \mathrm{d}t) \approx \rho_{\text{w}} A_{\text{c}}(0 + \mathrm{d}t)\, V_{\text{c}}(0)\mathrm{d}t. \tag{A 7}$$

Expressing the basic definition $a_{\text{w}} = \mathrm{d}V_{\text{w}}/\mathrm{d}t$ in a finite difference and using (A 6) and (A 7) yields

$$V_{\text{w}}(0 + \mathrm{d}t) \approx 0 + a_{\text{w}}(0 + \mathrm{d}t)\mathrm{d}t \approx \frac{F_{\text{BC}}}{M_{\text{w}}(0 + \mathrm{d}t)}\mathrm{d}t \approx \frac{F_{\text{BC}}}{\rho_{\text{w}} A_{\text{c}}(0 + \mathrm{d}t)\, V_{\text{c}}(0)}. \tag{A 8}$$

This result forms the basis for equations (4.1)–(4.3) used in §4.3.

A.4. Pressure inside the ventral cavity

The use of one-dimensional hydrodynamics allows a simple calculation of the pressure profile inside the mouth, which could be detected by mechanoreceptors just medial to each ventral groove (deBakker *et al.* 1997). Such a pressure calculation follows in a straightforward manner once the equations of motion (3.1), (3.2), (A 1) and (A 2) have been solved (Potvin 1999).

First, the internal fluid's continuity equation trivially demands that the entire internal flow moves at the same speed, in other words that V_w be the same for *all* slugs enclosed in the mouth. This is why the one-dimensional (incompressible) hydrodynamic approach pictures the motion of the slug train as being similar to that of a (dually tapered) solid rod. From that viewpoint, the Euler (i.e. momentum) equation for internal flow simplifies greatly, yielding

$$P(X_w + x, t) - P(X_w, t) = -\rho_w \frac{dV_w}{dt} x, \qquad (A\ 9)$$

with x being the location, with respect to a fixed point deep inside the throat, of the probe that would measure the pressure P at time t. Note that V_w rather than $(V_c - V_w)$ is being used in the time derivative, given the fact that the Euler equations were set up with coordinates defined relative to the fixed reference point on the shore (figure 13). Note also that the value of V_w at time t is calculated from the simultaneous solution of (3.1), (3.2), (A 1) and (A 2). Equation (A 9) entails that the differential pressure between the leading engulfed slug and any location x towards the mouth opening is directly proportional to both x and slug acceleration.

A simpler measure (i.e. one-dimensional) of the internal pressure environment, on the other hand, is that of the internal pressure *gradient* $\Delta P/\Delta X$ between the leading and trailing engulfed slugs, or, in other words, between a point near the opened mouth and one of the deepest water penetration into the mouth,

$$\frac{\Delta P}{\Delta X} \equiv \frac{P(X_w, t) - P(X_w + (X_c - X_w), t)}{X_c - X_w} = \rho_w \frac{dV_w}{dt}. \qquad (A\ 10)$$

This result is obtained from equation (A 9) by dividing both sides by $-x = -(X_c - X_w) \equiv \Delta X$. Here, the overall sign change makes the pressure gradient positive for what is expected in nature, i.e. for those cases for which the engulfed water is accelerated while moving in the same direction as the whale. Such a pressure gradient function thus depends only on time and provides a quick outlook of the internal pressure.

Finally, note that equation (A 9) could also be used to estimate $P(X_w + x, t)$ anywhere in the mouth, but only once the pressure $P(X_w + L_{max}^{long}, t)$ at the mouth is known. However, a rough estimate can be obtained if the (known) static pressure of the water just outside the mouth is used. Such information, together with the knowledge of the prescribed throat wall force $F_{tw}(t)$, could then be used to estimate a rough surface area over which this force is applied inside the cavity.

REFERENCES

Acevedo-Gutierrez, A., Croll, D. A. & Tershy, B. R. 2002 High feeding costs limit dive time in the largest whales. *J. Exp. Biol.* **205**, 1747–1753.

Bose, N. & Lien, J. 1989 Propulsion of a fin whale (*Balaenoptera physalus*)—why the fin whale is a fast swimmer. *Proc. R. Soc. B* **237**, 175–200. (doi:10.1098/rspb.1989.0043)

Brodie, P. F. 1993 Noise generated by the jaw actions of feeding fin whales. *Can. J. Zool.* (*Revue Canadienne De Zoologie*) **71**, 2546–2550. (doi:10.1139/z93-348)

Brown, S. G. & Lockyer, C. H. 1984 Whales. In *Antarctic ecology*, vol. 2 (ed. R. M. Laws), pp. 717–781. New York, NY: Academic Press.

Calambokidis, J., Schorr, G. S., Steiger, G. H., Francis, J., Bakhtiari, M., Marshall, G. & Oleson, E. 2008 Insights into the underwater diving, feeding, and calling behavior of blue whales from a suction-cup attached video-imaging tag (Crittercam). *MTS J.* **31**, 15–25.

Cochran, B. C., White, B. R. & Macha, J. M. 1991 Experimental investigation of added mass during parachute deceleration—preliminary results. In *11th AIAA Aerodynamic Decelerator Systems Technology Conference, San Diego, CA*, pp. 171–180.

Cooper, L. N., Sedano, N., Johansson, S., May, B., Brown, J. D., Holliday, C. M., Kot, B. W. & Fish, F. E. 2008 Hydrodynamic performance of the minke whale (*Balaenoptera acutorostrata*) flipper. *J. Exp. Biol.* **211**, 1859–1867. (doi:10.1242/jeb.014134)

Croll, D. A., Acevedo-Gutierrez, A., Tershy, B. R. & Urban-Ramirez, J. 2001 The diving behavior of blue and fin whales: is dive duration shorter than expected based on oxygen stores? *Comp. Biochem. Physiol. Mol. Integr. Physiol.* **129**, 797–809. (doi:10.1016/S1095-6433(01)00348-8)

deBakker, M. A. G., Kastelein, R. A. & Dubbeldam, J. L. 1997 Histology of the grooved ventral pouch of the minke whale, *Balaenoptera acutorostrata*, with special reference to the occurrence of lamellated corpuscles. *Can. J. Zool.* (*Revue Canadienne De Zoologie*) **75**, 563–567. (doi:10.1139/z97-069)

Desabrais, K. J. & Johari, H. 2003 Unsteady potential flow forces on an inflating parachute canopy. In *17th AIAA Aerodynamic Decelerator Systems Technology Conference, Monterey, CA*. Paper AIAA-2003-2144.

Doherr, K. 2003 Extended parachute opening shock estimation method. In *17th AIAA Aerodynamic Decelerator Systems Technology Conference and Seminar, Monterey, CA*. Paper AIAA-2003-2173.

Ford, J. K. B. & Reeves, R. R. 2008 Fight or flight: antipredator strategies of baleen whales. *Mammal Rev.* **38**, 50–86. (doi:10.1111/j.1365-2907.2008.00118.x)

Gaskin, D. E. 1982 *The ecology of whales and dolphins*. London, UK: Heinemann.

Goldbogen, J. A., Calambokidis, J., Shadwick, R. E., Oleson, E. M., McDonald, M. A. & Hildebrand, J. A. 2006 Kinematics of foraging dives and lunge-feeding in fin whales. *J. Exp. Biol.* **209**, 1231–1244. (doi:10.1242/jeb.02135)

Goldbogen, J. A., Pyenson, N. D. & Shadwick, R. E. 2007 Big gulps require high drag for fin whale lunge feeding. *Mar. Ecol. Progr. Ser.* **349**, 289–301. (doi:10.3354/meps07066)

Goldbogen, J. A., Calambokidis, J., Croll, D., Harvey, J., Newton, K., Oleson, E., Schorr, G. & Shadwick, R. E. 2008 Foraging behavior of humpback whales: kinematic and respiratory patterns suggest a high cost for a lunge. *J. Exp. Biol.* **211**, 3712–3719. (doi:10.1242/jeb.023366)

Gould, H. & Tobochnik, J. 1996 *An introduction to computer simulation methods*. New York, NY: Addison-Wesley.

Halsey, L. G., Butler, P. J. & Blackburn, T. M. 2006 A phylogenetic analysis of the allometry of diving. *Am. Nat.* **167**, 276–287. (doi:10.1086/499439)

Higuchi, H., Balligand, H. & Strickland, J. H. 1996 Numerical and experimental investigations of the flow over a disk undergoing unsteady motion. *J. Fluids Struct.* **10**, 705–719. (doi:10.1006/jfls.1996.0049)

Iversen, H. W. & Balent, R. 1951 A correlating modulus for fluid resistance in accelerated motions. *J. Appl. Phys.* **22**, 324–328. (doi:10.1063/1.1699949)

Kot, B. W. 2005 Rorqual whale surface-feeding strategies: biomechanical aspects of feeding anatomy and exploitation of prey aggregations along tidal fronts. MSc thesis, p. 80. University of California, Los Angeles.

Lambertsen, R. H. 1983 Internal mechanism of rorqual feeding. *J. Mammal.* **64**, 76–88. (doi:10.2307/1380752)

Lambertsen, R., Ulrich, N. & Straley, J. 1995 Frontomandibular stay of Balaenopteridae—a mechanism for momentum recapture during feeding. *J. Mammal.* **76**, 877–899. (doi:10.2307/1382758)

Lockyer, C. 1976 Body weights of some species of large whales. *ICES J. Mar. Sci.* **36**, 259–273. (doi:10.1093/icesjms/36.3.259)

Lockyer, C. H. 1981 Growth and energy budgets of large baleen whales from the Southern Hemisphere. In *Mammals in the seas*. FAO Fisheries Series, vol. 3, pp. 379–487. Rome, Italy: FAO.

Orton, L. S. & Brodie, P. F. 1987 Engulfing mechanics of fin whales. *Can. J. Zool.* (*Revue Canadienne De Zoologie*) **65**, 2898–2907.

Panigada, S., Zanardelli, M., Canese, S. & Jahoda, M. 1999 How deep can baleen whales dive? *Mar. Ecol.-Progr. Ser.* **187**, 309–311. (doi:10.3354/meps187309)

Pivorunas, A. 1977 Fibro-cartilage skeleton and related structures of ventral pouch of balaenopterid whales. *J. Morphol.* **151**, 299–313. (doi:10.1002/jmor.1051510207)

Pivorunas, A. 1979 Feeding mechanisms of baleen whales. *Am. Sci.* **67**, 432–440.

Potvin, J. 1999 Simple description of airflow characteristics inside an unfolding parachute. *J. Aircraft* **36**, 809–818. (doi:10.2514/2.2514)

Potvin, J. 2008 General mass capture model for swiftly opening parachutes. *J. Aircraft* **45**, 1689–1700. (doi:10.2514/1.35552)

Potvin, J., Peek, G. & Brocato, B. 2003 New model of decelerating bluff-body drag. *J. Aircraft* **40**, 370–377. (doi:10.2514/2.3103)

Sarpkaya, T. 1991 Method of analysis for flow around parachute canopies. In *11th AIAA Aerodynamic Decelerator Systems Technology Conference, Reston, VA*, pp. 1–17.

Sarpkaya, T. & Isaacson, M. 1981 *Mechanics of wave forces on offshore structures*. New York, NY: Van Nostrand Reinhold Company.

Spahr, H. R. & Wolf, D. F. 1981 Theoretical analysis of wake-induced parachute collapse. In *7th AIAA Aerodynamic Decelerator and Balloon Technology Conference, San Diego, CA*. Paper AIAA-81-1922.

Strickland, J. H. & Macha, M. 1990 Preliminary characterization of parachute wake recontact. *J. Aircraft* **27**, 501–506. (doi:10.2514/3.25311)

True, F. W. 1904 Whalebone whales of the western North Atlantic. *Smithson. Contrib. Knowledge* **33**, 1–332.

Vogel, S. 1994 *Life in moving fluids: the physical biology of flow*. Princeton, NJ: Princeton University Press.

Werth, A. J. 2007 Adaptations of the cetacean hyolingual apparatus for aquatic feeding and thermoregulation. *Anat. Rec.-Adv. Integr. Anat. Evol. Biol.* **290**, 546–568. (doi:10.1002/ar.20538)